

1 **PIPEJACKING CLOGGING DETECTION IN SOFT ALLUVIAL DEPOSITS USING**
2 **MACHINE LEARNING ALGORITHMS**

3

4 Xue-Dong Bai¹, Wen-Chieh Cheng^{2,3}, Brian B. Sheil⁴ and Ge Li¹

5

6

7 ¹PhD student, School of Civil Engineering, Xi'an University of Architecture and Technology,

8 Xi'an 710055, China. Email: baixuedong@xauat.edu.cn (X.-D. Bai), lige@xauat.edu.cn (G.

9 Li)

10 ²Professor, School of Civil Engineering, Xi'an University of Architecture and Technology,

11 Xi'an 710055, China. Email: w-c.cheng@xauat.edu.cn (W.-C. Cheng)

12 ³Shaanxi Key Laboratory of Geotechnical and Underground Space Engineering (XAUAT),

13 Xi'an 710055, China

14 ⁴RAEng Research Fellow, Department of Engineering Science, University of Oxford, U.K.

15 Email: brian.sheil@eng.ox.ac.uk (B.-B. Sheil)

16

17

18

19

20

21

22

23

24

25 Revision submission,

26 Main text word count: 7413

27 Tables: 3

28 Figures: 19

29 **ABSTRACT**

30 'Clogging' is a common issue encountered during tunnelling in clayey soils which can impede
31 tunnel excavation, cause unplanned downtimes and lead to significant additional project costs.
32 Clogging can result in a drastic reduction in performance due to reduced jacking speeds and
33 the time needed for cleaning if it cannot be fully mitigated. The data acquired by modern tunnel
34 boring machines (TBMs) have grown significantly in recent years presenting a substantial
35 opportunity for the application of data-driven artificial intelligence (AI) techniques. In this study,
36 a baseline assessment of clogging in slurry-supported pipejacking is performed using a
37 combination of TBM parameters and the semi-empirical diagram proposed in the literature.
38 The potential for one-class support vector machines (OCSVM), isolation forest (IForest) and
39 robust covariance (Robcov) to assess the tendency to clayey clogging is then explored in this
40 work. The proposed approach is applied to a pipejacking case history in Taipei, Taiwan,
41 involving tunnelling in soft alluvial deposit. The results highlight an exciting potential for the
42 use of OCSVM, IForest and Robcov to detect clogging during slurry-supported pipejacking.

43

44 **KEYWORDS:** support slurry; pipejacking; clayey clogging; jacking speed; cutterwheel torque

45 INTRODUCTION

46 Fine-grained soils have a strong influence on pipejacking performance due to their tendency
47 to trigger different issues (Tan and Wei 2012; Ong and Choo 2016; Soomro et al. 2020; Zhang
48 et al. 2020a), one of which is 'clogging'. Clogging denotes the adherence of fine-grained soils
49 to cutters at the cutterhead, openings on the cutting wheel, screw conveyor and/or conveyor
50 belt. Clogging can therefore cause unplanned downtimes and, consequently, a significant
51 increase in operation costs (Thewes and Burger 2005; Spagnoli et al. 2011a; Heuser et al.
52 2012; Hollmann and Thewes 2013; Thewes and Hollmann 2014; Zumsteg et al. 2016). For
53 pipejacking, clogging can be described as the attraction between soil particles and cutters and
54 the adhesion between water in the soil and the cutters (Fontaine 1954; Sass and Burbaum
55 2008; Kang et al. 2018, 2019). There are four potential mechanisms governing adhesion of
56 clay to a cutter, namely adhesion of clay particles on a cutter surface, inherent cohesion,
57 bridging of clay particles over a cutting wheel opening, and an inability for the clay to dissolve
58 in water (Thewes 1999; Jia 2004; Kang et al. 2019). Previous research has shown that
59 clogging caused by adhesion of clay to a cutter can significantly reduce shield tunnelling
60 performance (van Baalen 1999, 2001; Spagnoli et al. 2011b, 2012a,b, 2014; Zhang et al.
61 2018).

62 Various approaches have been proposed to evaluate the potential for clogging to occur such
63 as the use of plasticity index measurements, semi-empirical diagrams, and laboratory-based
64 drilling tests. Hu and Rostami (2020) described the importance of soil conditioning during
65 tunnelling and the role of soil rheology in tuning the desired characteristics of the conditioned
66 soil. Using a novel device, those authors established a relationship between soil rheological
67 parameters, soil type and conditioning parameters for soft ground tunnelling. Using a new
68 framework and new devices, Peila et al. (2015) noted that the effectiveness of a polymer in
69 clay conditioning is strongly dependent on the plasticity index of the clay. For low plasticity
70 clay, the use of polymers can cause an increase in the volume of foam needed because of
71 the water absorption effect of the polymer itself. However, this can also lead to a more
72 homogeneous conditioned soil with long-lasting mechanical properties. Alberto-Hernandez et
73 al. (2017) used the relationship between cohesion (soil-soil strength) and adhesion (soil-
74 structure strength) to evaluate clogging potential, though this method is limited to situations
75 where soil cohesion is greater than adhesion. Hollmann and Thewes (2013) reported relevant
76 factors for the development of clogging and presented a new classification diagram which
77 allows for the quantification of changes in the water content towards estimating changes in
78 the consistency of fine-grained soils under varying availabilities of water. Thewes and
79 Hollmann (2016) explored the risk of clogging in various ground conditions and for different
80 shield types and presented a summary of methods to characterise soil 'stickiness' and

81 laboratory experiments to assess clogging potential. A newly developed diagram for assessing
82 clogging risks for all types of shields and a new testing scheme for evaluating sedimentary
83 rocks in terms of clogging were also introduced. Feinendegen et al. (2010) recommended a
84 cone pull-out test to detect the adhesion/clogging propensity of a rock or soil, combined with
85 a newly developed scheme for classifying the clogging potential. Following an extended test
86 campaign using soils with different clay contents and minerals, de Oliveira (2018) developed
87 a new device which adds to the first method a kinetic energy impulse via dropping of the beater
88 from a certain height. This combination could give a more reliable evaluation of the potential
89 for clogging to occur along earth pressure balance (EPB) machine tunnel drives. Further, a
90 laboratory routine to characterise the clogging and fluidity of soils, including mixed soils by
91 considering different fractions of clay was proposed by de Oliveira (2019a,b,c). But this routine
92 can still be improved by doing this exercise of preliminary assessment and later backanalysis.

93 Kang et al. (2019) evaluated the clogging potential of mixed bentonite-kaolin specimens using
94 a combination of the semi-empirical diagram and the drilling test. Kang et al. (2019) also
95 investigated the dependence of the clogging potential on the plasticity indices of the mixtures.
96 The results revealed that mixtures with bentonite had a higher clogging potential than pure
97 kaolin and the drilling tests proved an effective means of quantifying clogging potential and
98 evaluating the performance of additives. Zumsteg et al. (2016) investigated the effect of clay
99 mineralogy and the composition of the supporting slurry on clogging potential using novel
100 'stickiness' tests including a 'mixing test' and a model tunnel boring machine (TBM) cutterhead
101 test. It was reported that increased slurry strength is likely to increase the possibility of clogging
102 for mixed face conditions. In contrast, polymer additives to slurry can achieve both high slurry
103 resistance with low clogging potential by protecting clay aggregate surface from penetration
104 of water (Zumsteg et al. 2016).

105 Although previous studies performed over the past decade have greatly enhanced our
106 understanding of the clogging process and the role of key influencing factors (Zumsteg et al.
107 2013; Ryu et al. 2019), the influence of clogging on the response of tunnelling parameters (e.g.
108 cutterwheel torque and jacking speed) remains unclear. Further, the prevention and mitigation
109 of clogging during shield tunnelling is still highly dependent on the operator's accumulated site
110 experience. The objectives of this paper are: (1) to characterise the response of tunnelling
111 parameters to the development of clogging during slurry-supported pipejacking, (2) to evaluate
112 the clogging potential using a combination of the existing pipejacking parameters and the
113 semi-empirical approach, and (3) to explore the feasibility for artificial intelligence techniques
114 to evaluate the clogging potential.

115

116 CRITICAL FACTORS FOR THE DEVELOPMENT OF CLOGGING

117 *Particle-size distribution*

118 The shear strength of coarse-grained soils (with less than 5% fines) is derived from
119 interparticle friction and geometrical interference (e.g. dilation, particle crushing, and
120 rearrangement) rather than cohesion and they, therefore, minimises clogging issues during
121 tunnel excavation. In contrast, coarse-grained soils (e.g. sands and gravel) with fines content
122 > 5% have been shown to increase the potential for clogging (Ni and Cheng 2010). In this
123 context, soil particles > 0.075 mm become part of the clogging material (i.e. causing the
124 blockage), whereas particles < 0.075 mm become ‘abrasive’ material (i.e. leading the wear of
125 cutting tools). On the other hand, fine-grained soils always promote clogging and a higher
126 concentration of fines content in the slurry during pipejacking (Tombacz and Szekeres 2006).
127 Thus, a comprehensive assessment of the particle size distribution is a prerequisite for a
128 rigorous evaluation of clogging potential.

129 *Soil plasticity and consistency*

130 Three water contents typically used to define the state of fine-grained clayey soils are the
131 natural water content ω_n , liquid limit ω_L and plastic limit ω_P . An increasingly popular means of
132 evaluating clogging potential is through a combination of the plasticity index $I_p (= \omega_L - \omega_P)$ and
133 the consistency index $I_c = (\omega_L - \omega_n)/(\omega_L - \omega_P)$. According to Thewes (1999), clayey soils with
134 $I_p > 20\%$ and $I_c = 0.75-1.25$ have the highest potential to cause clogging. However, more recent
135 investigations have shown that extensive clogging can even occur in clayey soils with $I_c =$
136 $1.25-1.50$ (Thewes 1999). Hollmann and Thewes (2013) examined 150 samples of “sticky”
137 material obtained from open and slurry-supported shield tunnelling projects. The samples
138 varied between very soft (23% of samples; $I_c = 0.4-0.5$), soft-medium (58%; $I_c = 0.5-0.75$) and
139 stiff (19%; $I_c = 0.75-1.0$) consistency. Laboratory test results reported by Feinendegen et al.
140 (2011) show good agreement with those documented by Hollmann and Thewes (2013).
141 Encountering clayey soils with “soft” consistency during tunnelling is, therefore considered
142 high-risk for the development of clogging. In contrast, clayey soils with stiff consistency is likely
143 to show relatively low clogging potential because of their lower ω_n , whereas clayey soils with
144 very soft consistency also have relatively low clogging potential since their reduced shear
145 strength is not high enough to resist the shear stresses exerted in the excavation chamber.

146 *Free water*

147 Free water, including groundwater inflow and water contained in bentonite slurry and the soil
148 conditioning agent, also plays an important role in clogging potential during tunnel excavation.
149 It is possible for cohesive soil with clay content > 10% to be transformed into clogging material.
150 However, the time taken to achieve this transformation is closely related to the natural soil

151 consistency and the availability of free water which, in turn, is dependent on the type of tunnel
152 excavation method. In slurry-supported shield tunnelling, the large amount of free water (due
153 to the use of bentonite slurry) leads to a higher clogging potential in clayey soils. The authors'
154 experiences are that even very stiff consistency clays can eventually be transformed to a soft
155 consistency. In contrast, in the case of open shield tunnelling the amount of groundwater
156 depends on both the inflow rate and construction downtime. Previously sticky clays in the
157 excavation chamber could transform into non-sticky material when their adhesion reduces
158 over time. Thus, it can be realised that the availability of free water must also be considered
159 when assessing the potential for clogging to occur during shield tunnelling.

160

161 **ASSESSMENT OF CLOGGING POTENTIAL**

162 *Methodology*

163 In this work, three slurry-supported pipejacking drives undertaken in the soft alluvial deposits
164 at Taipei, Taiwan were analysed. Following acquisition of the soil particle size distribution,
165 plasticity I_p and consistency index I_c , a baseline assessment of the clogging potential was
166 completed using existing pipejacking records, aided by the semi-empirical approach
167 (Hollmann and Thewes 2013). The time history of pipejacking performance parameters are
168 typically non-stationary which can lead to difficulties in the identification of patterns in the data.
169 Decomposition procedures can be used to alleviate this problem by disaggregating time series
170 data into feature-based sub-series where a weighted moving average dominates data features
171 retained in analysis and eliminates noises.

172 The large volume of data extracted by modern TBMs presents a substantial opportunity for
173 the application of data-driven anomaly detection (AD) techniques to identify patterns in the
174 data. Instead of simulating the measured system response, AD approaches accentuate
175 characteristics of the system by utilising information extracted from the measured data.
176 Evolutionary Polynomial Regression (EPR) has been drawn more attention because of its
177 more powerful ability in searching the target expression than artificial neural networks (ANNs)
178 and genetic programming (GP) (Gurocak et al. 2012; Alemdag et al. 2016; Yin et al. 2016).
179 Usually the global search for the best expression of the EPR equation is conducted using a
180 genetic algorithm (GA) over the values contained in the user defined vector of components.
181 For high dimensional problems, GAs, however, require a long period of computational time
182 and large memory (Deep and Thakur 2007a,b). Multivariate Adaptive Regression Splines
183 (MARS) primarily aims to organise relationships between a set of input variables and the target
184 dependent (Zhang et al. 2020c). MARS is a nonparametric statistical method based upon
185 'divide and conquer' strategy where the training datasets are partitioned into separate

186 piecewise linear splines of different gradients towards representing the integration of additive
 187 regression, recursive regression, spline regression and recursive partitioning regression.
 188 Compared with the regression AD algorithms, ‘unsupervised’ clustering AD algorithms are
 189 more appropriate to process unlabelled data since the measured data (i.e. the outputs) are
 190 not labelled in most of practical problems. Unsupervised clustering AD algorithms, applied to
 191 infer characteristics in data without reference to known labels, are popular for this reason and
 192 employed in this work. A myriad of approaches have been proposed in the literature (Zhang
 193 et al. 2020b,c); three of the more popular AD approaches are adopted for this study: (1) one-
 194 class support vector machines (OCSVM), (2) isolation forest (IForest) and (3) robust
 195 covariance (Robcov). The three AD methods are applied to all case histories where clogging
 196 was encountered to assess their ability to identify clogging behaviour during pipejacking.
 197 Baseline assessments are also undertaken to benchmark predictions determined using the
 198 AD techniques.

199 *One-class support vector machines*

200 Traditionally many classification problems attempt to solve the two or multi-class situation.
 201 The goal of the machine learning task is to discriminate between subclasses of a dataset using
 202 a ‘training’ portion of the data. One-class support vector machine (OCSVM) denotes the case
 203 where the data comprises only one class and the task is to identify whether new
 204 measurements belong to that class. Schölkopf et al. (2001) framed the OCSVM approach by
 205 considering the origin as the only member of the second class (Sheil et al. 2020). A hyperplane
 206 is constructed in the feature space to separate the dataset from the origin, using a maximal
 207 margin (Fig. 1). The hyperplane constructs the following classification rule:

$$f(x) = (\mathbf{w} \cdot x) + b \quad (1)$$

208 where \mathbf{w} = adjustable weight vector and b = bias. The objective is to obtain a function that
 209 gives the maximum margin between the data and the origin. To prevent the OCSVM classifier
 210 from overfitting, slack variables ξ_i are used to create a ‘soft margin’ which allows some
 211 datapoints to lie within the margin. The optimal separating hyperplane can be obtained by
 212 solving the following convex quadratic optimisation problem (Vapnik 1995):

$$\begin{aligned} \text{Minimise} \quad & \frac{1}{2} \|\mathbf{w}\|^2 + \frac{1}{\nu n} \sum_{i=1}^n \xi_i - \rho, \quad i = 1, 2, \dots, n \\ \text{Subject to} \quad & (\mathbf{w} \cdot \Phi(x_i)) \geq \rho - \xi_i, \quad i = 1, 2, \dots, n \quad \xi_i \geq 0 \end{aligned} \quad (2)$$

213 where n = number of observations, ρ = margin, and ξ_i = slack variable, which is penalised in
 214 the objective function for nonzero values. The $\|\mathbf{w}\|^2$ term in Eq. (2) is an L2 regularisation term

215 to minimise overfitting, and its relative importance is controlled by the parameter ν . As the
 216 outcome of the decision function relies only on the dot-product of the vectors in the feature
 217 space, an explicit mapping to the feature space is not necessary. The ‘kernel trick’ is often
 218 adopted which allows the dot-product to be substituted by kernel functions. The decision
 219 function (i.e. classification rule) for a datapoint x can therefore be written as:

$$f(x) = \text{sign} \sum_{i=1}^{N_{sv}} \alpha_i K(x_i, x) - \rho \quad (3)$$

220 where α_i = Lagrange multiplier and N_{sv} = number of support vectors. Every α_i which is > 0 is
 221 weighted in the decision function to ‘support’ the vector machine. Popular selections for the
 222 kernel include linear, polynomial, radial basis function (RBF) and sigmoid. RBF is the kernel
 223 that was selected here:

$$K(x_i, x) = \exp\left(-\gamma \|x_i - x_j\|^2\right) \quad (4)$$

224 where γ = kernel parameter, which is the width of the RBF and typically varies between 0 and
 225 1, and $\|x_i - x_j\|$ = dissimilarity measure.

226 *Isolation forest*

227 The IForest is a non-parametric method that constructs classification models in the form of a
 228 ‘tree’ structure. An isolation forest, as the name suggests, is an ensemble learning method
 229 that operates by constructing n_{tree} isolation trees and aggregating the results, as illustrated in
 230 Fig. 2. The IForest approach detects anomalies by randomly partitioning the data. Partitions
 231 are created by randomly selecting a feature and then randomly producing a split value
 232 between the maximum and the minimum value of the feature. Partition creation continues until
 233 all datapoints are isolated; in most cases a limit is placed on the maximum number of partitions.
 234 Multiple training datasets are produced by sampling with replacement randomly from the
 235 original dataset, and anomalies are ultimately identified by sorting datapoints according to their
 236 corresponding path lengths (Sheil et al. 2020). For a dataset of size n , the average, $c(n)$, of
 237 each path length, $h(x)$, is calculated as:

$$c(n) = 2H(n - 1) - \left(\frac{2(n - 1)}{n}\right) \quad (5)$$

238 where $H(i)$ = harmonic number (i.e. $H(i) = \ln(i) + a$, where a is Euler-Mascheroni constant).
 239 The IForest anomaly score (IF) is then defined as:

$$IF(x, n) = 2 \frac{E(h(x))}{c(n)} \quad (6)$$

240 where $E(h(x))$ = average of $h(x)$ from a collection of isolation trees. A value of $IF > 1.0$ is
241 classified as anomalous in this study (Liu et al. 2012).

242 *Robust covariance*

243 The robust covariance ('Robcov') approach was first proposed by Rousseeuw (1984). The
244 concept is to find a given proportion of 'good' observations which are not outliers and compute
245 their empirical covariance matrix. Then this empirical covariance matrix is rescaled towards
246 compensating the performed selection of observations (namely, consistency step). Having
247 computed the Minimum Covariance Determinant (MCD) estimator, one can give weights to
248 observations according to their Mahalanobis distance md , leading to a reweighed estimate of
249 the covariance matrix of the dataset (namely, reweighting step). For data following a Gaussian
250 distribution, the distance of an observation x_i to the mode of the distribution can be computed
251 using its md as follows:

$$md(\mu, \Sigma)(x_i)^2 = (x_i - \mu)' \Sigma^{-1} (x_i - \mu) \quad (7)$$

252 where μ = location of the underlying Gaussian distribution and Σ = covariance of the underlying
253 Gaussian distribution. As the usual covariance maximum likelihood estimate is very sensitive
254 to the presence of outliers in the data, a more robust estimator of covariance is required to
255 minimise the influence of 'erroneous' observations such that md accurately reflect the true
256 organisation of the observations (Fig. 3). Larger values of md denote anomalous observations.

257 *Feature selection*

258 Decomposition techniques, proposed by Persons (1919), isolate salient features of a dataset
259 (e.g. trend (seasonal) component and periodic component). Seasonal-trend decomposition
260 using Loess smoothing (STL; Cleveland et al. 1990) is one of the most popular decomposition
261 techniques and is also used here to partition the global series into three additive components
262 as follows:

$$y_t = P_t + T_t + R_t \quad (8)$$

263 where P_t = periodic component, T_t = trend component and R_t = residual component. In this
264 work, two feature variables are considered for the application of OCSVM, IForest and Robcov,
265 namely, the residual and trend components of the density of support slurry ρ , the cutterwheel
266 torque T_c , and the jacking speed V . The periodic component P_t was derived based upon a
267 minimum length of 3 m (i.e. three datapoints). Since the current supplied to the cutterwheel of
268 shield machine is used as a proxy for cutterwheel torque, the residual and trend torque
269 components are, therefore, plotted in 'Amps'.

270

271 **IMPLEMENTATION**

272 *Data screening*

273 As all case histories involved periods of tunnelling in gravel, the corresponding datapoints
274 were first filtered out of the datasets. The authors' previous research suggests $T_c > 15$ Amp
275 and $V \geq 100$ r/min correspond to tunnelling in gravel and they may vary between projects with
276 different geology (Cheng et al. 2017). These data were therefore filtered out from the dataset
277 such that all datapoints pertain to tunnelling in clayey soil. The data was logged at 2 m intervals
278 of jacked distance to capture the clogging-induced decline in V .

279 *Data scaling*

280 The OCSVM, IForest and Robcov algorithms were implemented using the Python module
281 *Scikit-learn* (Pedregosa et al. 2011). All data were scaled using a 'min-max scaler' such that
282 each feature varies between 0 and 1 (Masters 1993). Thus, given a set of input data $x_1,$
283 x_2, \dots, x_n , the scaled dataset z_1, z_2, \dots, z_n will be:

$$z_i = \frac{x_i - x_{min}}{x_{max} - x_{min}} \quad (9)$$

284 where *min* and *max* are our specified minimum and maximum values of the range to scale.
285 This pre-processing maximises the efficiency and performance of the learning process and
286 equalises the importance of the input dataset.

287 *Confusion matrix*

288 There are four possible outcomes from the analysis, commonly summarised in a 'confusion
289 matrix': (a) true positive (TP – system correctly identified clogging behaviour), (b) false
290 negatives (FN – system has failed to detect clogging behaviour), (c) false positives (FP –
291 system has erroneously detected clogging behaviour) and (d) true negatives (TN). The four
292 outcomes were considered here to evaluate the performance of the AD approaches using the
293 discovery rate (DR), or true positive rate, and the false alarm rate (FAR), or false negative
294 rate.

$$DR = \frac{TP}{TP + FN} \quad (10)$$

$$FAR = \frac{FP}{TN + FP} \quad (11)$$

295

296 **PIPEJACKING DRIVES**

297 *Project overview*

298 Fig. 4a shows the location of four drives in the soft alluvial deposits located in the Shulin district
299 in Taipei County, Taiwan. Due to the data completeness, three (drives B, C and D) out of the
300 four drives were selected for the present analyses and measured 126 m, 75 m and 102 m in
301 length respectively and were located approximately 10.5 m below ground level. The tunnelling
302 was undertaken using a slurry-supported shield machine with a 1.5 m diameter cutterhead. A
303 30 mm overcut in the annulus area was created using the 1 m long, 1.44 m wide trailing
304 concrete pipe. Each pipe weighed 12.6 kN. To minimise the frictional resistance between the
305 pipe string and surrounding soil, a highly viscous lubricant with Marsh cone viscosity of 38
306 mins was injected into the overcut annulus.

307 *Engineering Geology*

308 The geological profile as determined from four geologic boreholes BH1~4 adjacent to the four
309 drives is shown in Fig. 4b. While the soil properties profile as evaluated from both the field and
310 laboratory tests is shown in Fig. 5. It can be observed from Fig. 6 that drives B, C and D were
311 located within gravel and sand in the main. The soils are also classified as clayey gravel and
312 clayey sand for certain sections of drives B, C and D. The minor clay fraction plays a leading
313 role in the macroscale mechanical properties of the clayey gravel or clayey sand. In light of
314 this, the consistency of the clay particles constituted to the clayey gravel would be assessed
315 using a combination of the semi-empirical approach and the machine learning technologies.
316 The phreatic surface is located at a depth of approximately 4.5 m below ordnance datum
317 (BOD). Additional details on the project are available in Cheng et al. (2017, 2018, 2019a,b).

318

319 **RESULTS AND DISCUSSION**

320 *Baseline assessment results*

321 To benchmark predictions, a baseline assessment of clogging potential during pipejacking in
322 the clayey soils was completed using measurements of the support slurry density ρ , jacking
323 speed V , and cutterwheel torque T_C , in conjunction with the semi-empirical approach. During
324 pipejacking in clayey soils, the cutterwheel is pressed into the cutting face and the plastically
325 deformable soil is pushed to both sides in the form of 'lumps'. Water in support slurry can
326 transform the consistency of the cut lumps into a sticky consistency. In this context, uncritical
327 soils turn into sticky material, and parts of the fines content contained in the cut lumps or the
328 soil at the cutting face may disintegrate and accumulate in the support slurry. The negative
329 impacts, induced by the disintegrated fines content, only occur at the final stage of the support
330 slurry flushing process. However, the clogging, induced by the sticky material, happens

331 throughout process from the excavation at the cutting face (i.e. primary clogging) up to
332 separation and transport for disposal (i.e. secondary clogging). When clogging occurs, there
333 is a substantial reduction in V and there are also negative impacts on the cutterwheel torque
334 T_C due to the mechanical forces arising from the excavation-transport-disposal process.
335 Clogging also has a negative impact on the density of support slurry ρ ; very high ρ after a
336 flushing process may correspond to the presence of clayey soils in the support slurry (in
337 suspension or cut lumps). In contrast, there is a substantial reduction in ρ after the flushing
338 process for silty soils. Increasing the jacking force F_T is a common technique adopted by shield
339 operators to overcome clogging issues but this is not always proportional relation to the
340 severity of clogging. It is therefore likely that clogging is accompanied by a substantial
341 reduction in the jacking speed V , an increase in the cutterwheel torque T_C and high ρ after the
342 flushing process.

343 At drive B, the clayey gravel at jacking distances of 20-26 m, 45-65 m, 89-111 m, and 122-
344 126 m may pose a risk of clogging (see Fig. 7a). Although the value of V corresponding to
345 jacking distances of 45-65 m and 122-126 m show significant fluctuations, the variations in T_C
346 were not significant. These results indicate that the consistency of the excavated material was
347 not critical for clogging and its shear strength was not capable of withstanding the mechanical
348 forces exerted during the transport-disposal process. Further, ρ after slurry flushing was
349 measured to be significantly below the threshold of 12.6 kN/m^3 , which also corresponds to
350 higher content of silt and low clogging potential, as shown in Fig. 7b. For the section
351 corresponding to a jacking distance of 89-111 m, the variations in T_C also showed only slight
352 changes despite V reducing to below 30 r/min on three separate occasions. Corresponding
353 values of ρ were again significantly below the 12.6 kN/m^3 threshold (see Fig. 7b) indicating
354 that the soil consistency was not critical for clogging. In contrast, V , corresponding to a jacking
355 distance of 20-26 m, substantially reduced from 112.5 r/min to below 30 r/min despite the
356 discontinuous variations in T_C . It is noteworthy that ρ measured at 12.2 kN/m^3 (the highest of
357 ρ observed in this study), which is derived right after slurry flushing and close to the threshold
358 of 12.6 kN/m^3 . This phenomenon indicates that the excavation was undertaken in the clayey
359 soil and the spoil with high ρ , induced by the inclusion of clayey soil, caused some difficulty in
360 transporting the spoil towards leading to the inability to secure the jacking speed. Therefore,
361 tunnelling through this section was recognised as a relatively high risk of clogging.

362 For drive C, clayey gravels were encountered at jacking distances of 35-37 m, 41-53 m, 57-
363 64 m, 67 m, 70 m, and 72-73 m, as shown in Fig. 8a. At jacking distances of 67 m, 70 m, and
364 72-73 m, V was measured to be 50 r/min while T_C measurements reached a maximum of 20
365 Amp. Further, ρ dropped to as low as 9.9 kN/m^3 following slurry flushing, which also indicates
366 a higher content of silt, as shown in Fig. 8b. These results suggest low clogging risk in these

367 sections. In contrast, at jacking distances of 35-37 m, 41-53 m, and 57-64 m the measured
368 value of V increased to 137.5 r/min despite the similarly high values of T_C (25 Amp). In addition,
369 ρ measured significantly below 12.6 kN/m³ except at a jacking distance of 50 m where ρ =
370 11.6 kN/m³, as shown in Fig. 8b. It is worth noting that a decrease in V , accompanied by an
371 increase in T_C , occurred at jacking distance of 59-63 m, which was the result of a buried
372 wooden log strike, rather than clogging.

373 At drive D, six sections of the drive involved tunnelling in clayey gravel and were therefore
374 considered for analysis (jacked distances of 18-22 m, 26-47 m, 50 m, 55-62 m, 66-76 m, 81-
375 99 m in Fig. 9a). At a jacking distance of 18-22 m, while V and T_C were relatively constant, ρ
376 was measured to be 12.3 kN/m³ (Fig. 9b), indicating a higher content of clay soil and therefore
377 a higher tendency to clog. The section of clayey gravel at 50 m jacking distance was too short
378 to cause clogging issues. Although no data were available for ρ for a jacking distance of 55-
379 62 m, changes in V and T_C were not commensurate with clogging suggesting a low clogging
380 risk. For the section 83-99 m, V reduced to 35 r/min, T_C increased to 2.5 Amp and ρ was
381 measured to be 11.3 kN/m³ (see Figs. 9a and 9b) indicating low clogging risk. V and T_C both
382 showed decreasing trends while tunnelling through a jacking distance of 66-76 m, implying
383 that the material consistency could not withstand the mechanical forces exerted during the
384 excavation-transportation-disposal process. Compared to the jacking distance of 81-99 m,
385 there was comparatively less tendency for clogging at a jacking distance of 66-76 m even
386 though ρ was measured as 12.1 kN/m³. However, a high clogging risk was identified for a
387 jacking distance of 26-47 m due to the reduction in V (from 62 r/min to 25 r/min) and the
388 increase in ρ (from 9.9 kN/m³ to 12 kN/m³).

389 The use of the semi-empirical approach is also considered part of the baseline assessment of
390 clogging potential. Avunduk and Copur (2018) reported that specimens extracted from the
391 excavated material of a earth pressure balance (EPB) TBM, used in an Istanbul utility tunnel
392 project, were classified as low-plasticity clay (CL) or high-plasticity clay (CH) and characterised
393 by $I_p = 19-31\%$ and $I_c = 0.23-0.91$. Tokgöz (2016) analysed a total of 264 EPB-TBM excavation
394 performance data, when subjected to fine-grained sedimentary materials with $I_p = 40-68\%$ and
395 $I_c = 0.64-0.98$. The results revealed that F_T and T_C both increase while V decreases with
396 increasing I_p and I_c , and that the increase in T_C can be explained by the higher shear strength
397 of the clogging material. Further, one can deduce that the effect of fine-grained materials on
398 V mainly depends upon the clay morphology which affects specific surface area (SSA) and
399 then free water adsorption capability, and an appropriate designed soil conditioning chemical
400 is crucial to prevent clogging and adhesion-related problems. In this study, the fine-grained
401 soil specimens were extracted from nearby geological boreholes (Cheng et al. 2017) and from
402 those in Tamshui T1 area (Woo and Moh 1990) and their clogging potentials, as defined by

403 Hollmann and Thewes (2013), and those reported in the literature (Tokgöz 2016; Avunduk
404 and Copur 2018) were plotted in the universal classification diagram, as shown in Fig. 10. It
405 can be seen that I_p and I_c for the clayey soils spread over the worksite and Tamshui T1 area
406 are in the ranges of 8.3-12.9 and 0.27-0.60 respectively, hence substantiating all the
407 specimens of clogging material with predominantly high and/or little clogging potentials. The
408 results using the semi-empirical approach are in line with the authors' observations
409 corresponding to jacking distances of 20-26 m at drive B and 26-47 m at drive D.

410 *Machine learning results*

411 In this and subsequent sections, only drives B and D with a risk of clogging were analysed
412 and discussed. The performance results of AD approaches using the transformed slurry
413 density space are shown in Figs. 11 and 12. At drive B, all three AD approaches provided one
414 TP at 21 m jacking distance, with $R_t = 1.0$ and $T_t = 1.0$ (Fig. 11). There were two FPs
415 corresponding to jacking distances of 31 m and 41 m. At drive D, Robcov and IForest gave
416 one TP at 38 m jacking distance, whereas OCSVM provided one FN at 38 m jacking distance
417 (Fig. 12). There were two FPs (i.e. 65 m and 79 m) distributed on the right hand side of the
418 feature space (large R_t) and the other FP (i.e. 75 m) distributed on the left (small R_t). The
419 performance results of AD approaches using the transformed maximum torque space are
420 shown in Figs. 13 and 14. At drive B, IForest and OCSVM produced one TP at 24 m jacking
421 distance (Fig. 13). While Robcov provided one FN at 24 m jacking distance. There were four
422 FPs (i.e. 110-119 m) positioned on the bottom (small T_t) in the feature space and another one
423 FP (i.e. 10 m) distributed on the top right corner (large R_t and T_t). The other two (i.e. 54 m and
424 90 m) sat on the left (small R_t). At drive D, OCSVM and Robcov produced one TP at 38 m
425 jacking distance. IForest provided one FN at 38 m jacking distance (Fig. 14). There was one
426 FP (i.e. 89 m) distributed on the right (large R_t). The other three FPs (i.e. 19 m, 72 m and 73
427 m) sat on the top left corner (small R_t and large T_t) and the bottom left corner (small R_t and T_t)
428 as well as the bottom right corner (large R_t and small T_t) respectively. The performance results
429 using the transformed jacking speed space are shown in Figs. 15 and 16. At drive B, IForest
430 produced three datapoints at 20-26 m jacking distance. Robcov and OCSVM gave two
431 datapoints at 20-26 jacking distance. There were two FPs (i.e. 35 m and 49 m) distributed on
432 the top right corner (large R_t and T_t) in the feature space and another one FP (i.e. 36 m)
433 positioned on the top left corner (small R_t and large T_t) (Fig. 15). The other two FPs (i.e. 6 m
434 and 11 m) sat on the right (large R_t) and the left (small R_t) respectively. At drive D, OCSVM
435 and Robcov produced one datapoint (i.e. 39 m) at 26-47 m. IForest provided one FN (i.e. 39
436 m) at 26-47 m. There were three FPs (i.e. 62 m, 81 m and 82 m) distributed on the top right
437 corner (large R_t and T_t) in the feature space and another three (i.e. 57 m, 67 m and 68 m) sat

438 on the bottom left corner (small R_t and T_t) (Fig. 16). The other two FPs (i.e. 75 m and 83 m)
439 distributed on the top left corner (small R_t and large T_t).

440 *Discussion*

441 Measurements of ρ , T_C and V and their difference to 'nearby' datapoints can significantly affect
442 the assessment of clogging potential. There are two behaviours that address the formation of
443 clogging in this work: (1) absolute values of ρ , T_C and V , influence T_t and (2) the difference
444 between 'current' measurements of ρ , T_C and V from nearby datapoints influence R_t . For
445 brevity, only the typical assessment results using the density of support slurry ρ , the
446 cutterwheel torque T_C and the jacking speed V are discussed in sequence as follows. The
447 lower and upper limits of ρ corresponded to 10.8 kN/m³ and 12.2 kN/m³ respectively at drive
448 B and to 9.8 kN/m³ and 12.8 kN/m³ respectively at drive D. At drive B, the formation of FP at
449 41 m jacking distance was attributed to $T_t = 0$, induced by $\rho = 10.9$ kN/m³ dropping significantly
450 below the threshold of 12.6 kN/m³. Similarly, the FP at 65 m distance of drive D was formed
451 due to $T_t = 1.0$ and $R_t = 0.87$, induced by $\rho = 12.1$ kN/m³. These results can be categorised
452 into the 'type-1 behaviour'. In contrast, FP at 31 m distance of drive B was formed by $R_t = 0$,
453 induced by a decline in ρ to 10.8 kN/m³ from 12.2 kN/m³ at 21 m jacking distance. The higher
454 ρ from the nearby datapoint (i.e. 21 m distance) increased T_t and this, in turn, lowered R_t to 0.
455 At drive D, FP at 79 m jacking distance was produced as a result of $R_t = 1.0$, induced by an
456 increase in ρ to 11.3 kN/m³ from 10.1 kN/m³ at 75 m distance. The lower ρ from the adjoining
457 datapoint (i.e. 75 m distance) lowered T_t to approximately 0 and this, in turn, increased R_t to
458 1.0. These results can, therefore, be categorised as 'type-2 behaviour'.

459 The maximum of T_C (termed $T_{C,max}$ hereafter) varied from 65 Amp to 80 Amp at drive B,
460 whereas it varied between 45 Amp to 55 Amp at drive D. The main cause to lead to FP at 110
461 m jacking distance of drive B was due to $T_t = 0$, induced by $T_{C,max} = 65$ Amp (lower limit). $T_{C,max}$
462 from surrounding datapoints was similar and the impact on R_t was minimal. The FP at 26 m
463 jacking distance of drive D was caused by $T_t = 1.0$ from $T_{C,max}$ hitting the upper limit of 55 Amp.
464 Surrounding datapoints of similar $T_{C,max}$ produced a 'platform' leading to a negligible impact
465 on R_t . These results can therefore be classed as type-1 behaviour. In contrast, the leading
466 cause to form a FP at 10 m jacking distance of drive B was because of $R_t = 1.0$, induced by
467 $T_{C,max} = 80$ Amp (upper limit). $T_{C,max} = 70$ Amp from the nearby datapoints, i.e. 9 m and 11 m
468 jacking distance, lowered T_t to 0.75. This, in turn, increased R_t to 1.0. A FP at 89 m distance
469 of drive D was formed by $R_t = 1.0$, induced by $T_{C,max} = 55$ Amp (upper limit). Nearby datapoints
470 that are featured with $T_{C,max} = 45$ Amp (lower limit) increased R_t to 1.0 by lowering T_t to 0.4.
471 The above two instances can therefore be classed as the type-2 behaviour.

472 The difference in V measurements (termed ΔV hereafter) varied between -37.5-47.5 r/min and
473 -55-65 r/min for drives B and D respectively. A negative value of ΔV represents a descending
474 tendency in V , while a positive value indicates an ascending tendency in V . A FP at 35 m
475 jacking distance of drive B ($R_t = 0.98$ and $T_t = 1.00$) was triggered by $\Delta V = 47.5$ r/min (upper
476 limit). In addition, the FP at 57 m distance of drive D ($R_t = 0.02$ and $T_t = 0$) was caused by ΔV
477 reaching the lower limit of -55 r/min, indicating type-1 behaviour. The FP at 49 m jacking
478 distance of drive B ($R_t = 0.97$ and $T_t = 0.84$) was due to $\Delta V = 37.5$ r/min. $\Delta V = 0$ r/min from
479 48 m distance lowered T_t to 0.84 and this, in turn, increased R_t to 0.97. The FP at 83 m distance
480 of drive D was formed due to $R_t = 0$ and $T_t = 0.66$, induced by $\Delta V = -10$ r/min. $\Delta V = 55$ r/min
481 from 82 m distance increased T_t to 0.66, lowering R_t to 0 indicating type-2 behaviour. Table 2
482 summarises the R_t and T_t of datapoints and their behaviour in relation to clogging identification.
483 Datapoints distributed in quadrant II (high R_t and T_t) could produce outlier formed by a
484 clogging-induced increase in the density of support slurry or the cutterwheel torque, while
485 datapoints distributed in quadrant III (low R_t and T_t) could lead to outlier produced by a
486 clogging-induced decline in the jacking speed (see Fig. 17). Although the decision boundary
487 established by the IForest approach presented in an irregular shape which has not been seen
488 from the other two AD approaches and was proven rather sensitive to clogging behaviour, it
489 performed the worst amongst the AD approaches (Table 3). TBM or shield machines,
490 equipped with such an integrated AD system, can be useful to introduce countermeasures in
491 advance of clogging during drives in clayey soils.

492 For clay soils with low to medium clogging potential, the risk of adhesion is evaluated to be
493 low, according to the practical experience of the authors. However, a risk of clogged openings
494 remains throughout the spoil transport and disposal processes, depending upon the
495 consistency of the material. A clay with medium to high clogging potential can adhere to all
496 parts of the machine. Fig. 18 shows the clay soil adhered to the cutterwheel of machine to
497 produce clayey clogging at 20-26 m distance of drive B. The field observation locates where
498 the clayey clogging occurs and is in line with the clogging baseline assessment using the semi-
499 empirical approach. The Seasonal-Trend decomposition procedure using Loess successfully
500 accentuates the characteristics of data in response to the development of clayey clogging
501 towards allowing the 'slurry density' and 'maximum torque' as well as 'jacking speed' anomaly
502 detectors to detect the clayey clogging. The results obtained from this work provide evidence
503 in proving the reliability of the proposed approach and providing some guideposts as follows
504 for reducing the potential of clayey clogging while tunnelling in soft ground. To use a slurry-
505 supported shield machine in such a soil, small soil chips, narrow passages for the transport of
506 a clay chip from the cutting face to the support slurry line, sharp angles applied to the
507 excavation chamber and clay agglomerations in areas prone to material settlement should be

508 avoided. Therefore, generation of large soil chips to reduce the adhesion-prone surface of the
509 cut lump is essential to prevent the development of clogging. Further, optimised passages,
510 rounded angles and turbulence (namely, flushing nozzles and agitator) in areas which are
511 prone to material settlement should also be considered. Moreover, manipulating the ratio of
512 the suspension flow rate to the volume of cut lump gives a benefit in preventing clay from
513 accumulation.

514 Human factor is deemed as a crucial factor in anomaly detection for tunnel construction. The
515 authors have also noted that the torque variation, while pipejacking in 51-58 m distance at
516 drive B, is more distinct than other distances of same soil layer, implying that the human factor
517 may intervene the operation of tunnel boring machine and try to lift the machine out of the fine
518 grained soils by imposing 'breakout' cutterwheel torque. The other distinct variation in torque
519 occurs when jacking in 33-35 m distance at drive D. This is not due to the presence of the fine
520 grained soils but to the presence of the gravel. Despite the breakout torque present in 51-58
521 m distance at drive B, one of the advantages for the use of artificial intelligence technologies
522 is to accentuate patterns in the data and subsequently disaggregate time series data into
523 (stationary) feature-based sub-series towards preventing the accuracy of anomaly detection
524 from disturbing by unusual data induced by, for example, human factor.

525 A real-time anomaly detection (AD) scheme for tunnel construction has been proposed
526 following this work, as shown in Fig. 19. Three parts comprising acquisition of real-time data,
527 data pre-processing and clayey clogging assessment are integrated in the real-time AD
528 scheme. The real-time tunnelling data are collected by modern tunnel boring machine,
529 followed by the data pre-processing including data filtering, decomposition, feature selection
530 and scaling. The semi-empirical approach requires a measurement of the natural water
531 content, liquid limit and plastic limit to assess the development of clayey clogging and it cannot
532 be executed in a real time manner. Alternatively, we treat the modern tunnel boring machine
533 as a 'sensor' and the measured cutterwheel torque (T) can be converted to the tangential
534 adhesion stress (τ_t) towards establishing its relation with the thrust force σ_n (normal pressure).
535 This relation can then be used to determine the tangential strength τ and extended by taking
536 the water content of clayey soil into account. To this end, preliminary laboratory tests should
537 be conducted to investigate the change in τ with the water content. The real-time AD scheme,
538 assisted by the proposed anomaly detectors, can thus be realised, alarming the operator of
539 machine and reducing the potential of clogging while tunnelling in soft ground.

540

541 **CONCLUSIONS**

542 This paper has established a baseline assessment of clogging potential during slurry-
543 supported pipejacking using a combination of existing tunnelling parameters and the semi-
544 empirical approach and examined the potential for the use of anomaly detection approaches
545 to assess clogging potential. Based on the results and discussion, some main conclusions can
546 be drawn as follows:

- 547 (a) Pre-process procedures including data screening and a seasonal-trend decomposition
548 using Loess smoothing were utilised to transform the density of support slurry-distance
549 relationship, the maximum cutterwheel torque-distance relationship and the jacking
550 speed-distance relationship into stationary features for the application of anomaly
551 detection approaches. For the drives considered in this paper, two feature variables,
552 namely, the residual and trend components were found to be most effective in
553 accentuating the presence of anomalous (clogging) behaviour.
- 554 (b) The baseline assessment of clogging potential suggested there was a comparatively
555 high tendency for clogging to occur during pipejacking at jacking distances of 20-26 m
556 for drive B and 26-47 m for drive D. The assessment of anomalous behaviour using
557 the AD approaches indicated that the density of support slurry and the maximum
558 cutterwheel torque as well as the jacking speed provide an effective means to
559 assessing the risk of clogging. Even though the IForest approach established a
560 decision boundary that was most sensitive to anomalous behaviour, it performed the
561 worst amongst the AD approaches.
- 562 (c) Two behaviours that address the formation of clayey clogging were identified: (1)
563 absolute values of ρ , T_C and V , influence T_t and (2) the difference between 'current'
564 measurements of ρ , T_C and V from nearby datapoints influence R_t . The proposed real-
565 time anomaly detection scheme can be of great benefit to reduce the potential of
566 clogging during drives in clayey soils.
- 567 (d) Although the AD approaches have shown promising performance for assessing the
568 clogging potential during slurry-supported pipejacking, further validation regarding the
569 applicability of density of support slurry, maximum cutterwheel torque and jacking
570 speed to assess the tendency to clayey clogging is deemed necessary. In addition,
571 performance of the AD approaches requires to be examined when subjected to data
572 from drives with different geological conditions, construction techniques and shield
573 machine geometries.

574

575 **ACKNOWLEDGEMENTS**

576 The authors convey their thanks and sincerely acknowledge financial supports from the
577 Special fund for Basic Scientific Research of Central Colleges, Chang'an University, under
578 Grant No. 300102269502. The third author is funded by the Royal Academy of Engineering
579 under the Research Fellowship Scheme.

580

581 **DECLARATION OF COMPETING INTEREST**

582 The authors declare that they have no known competing financial interests or personal
583 relationships that could have appeared to influence the work reported in this paper.

584

585 **AUTHORSHIP CONTRIBUTION STATEMENT**

586 **Xue-Dong Bai**: Data curation, Formal analysis, Validation, Software, Writing - original draft.

587 **Wen-Chieh Cheng**: Conceptualization, Methodology, Writing - review & editing, Supervision,
588 Funding acquisition. **Brian B. Sheil**: Writing - review & editing. **Ge Li**: Data curation, Formal
589 analysis, Validation, Writing - original draft.

590 **REFERENCES**

- 591 Alberto-Hernandez, Y., Kang, C., Yi, Y., Bayat, A., 2017. Mechanical properties of clayey soil
592 relevant for clogging potential. *International Journal of Geotechnical Engineering*, 1-8.
593 doi: 10.1080/19386362.2017.1311086
- 594 Alemdag, S., Gurocak, Z., Cevik, A., Cabalar, A.F., Gokceoglu, C., 2016. Modeling
595 deformation modulus of a stratified sedimentary rock mass using neural network, fuzzy
596 inference and genetic programming. *Engineering Geology* 203, 70-82.
- 597 Breunig, M.M., Kriegel, H.P., Ng, R.T., Sander, J., 2000. LOF: Identifying density-based local
598 outliers. In Vol. 29 of ACM SIGMOD record, 93-104. New York: Association for
599 Computing Machinery.
- 600 Cheng, W.C., Ni, J.C., Shen, J.S., Huang, H.W., 2017. Investigation into factors affecting
601 jacking force: a case study. *Proceedings of the Institution of Civil Engineers-
602 Geotechnical Engineering*, 170(4): 322-334.
- 603 Cheng, W.C., Ni, J.C., Arulrajah, A., Huang, H.W., 2018. A simple approach for characterising
604 tunnel bore conditions based upon pipe-jacking data. *Tunnelling and Underground
605 Space Technology*, 71: 494-504.
- 606 Cheng, W.C., Ni, J.C., Huang, H.W., Shen, J.S., 2019b. The use of tunnelling parameters and
607 spoil characteristics to assess soil types: a case study from alluvial deposits at a
608 pipejacking project site. *Bulletin of Engineering Geology and the Environment*, 78:
609 2933-2942.
- 610 Cheng, W.C., Wang, L., Xue, Z.F., Ni, J.C., Rahman, M., Arulrajah, A., 2019a. Lubrication
611 performance of pipejacking in soft alluvial deposits. *Tunnelling and Underground
612 Space Technology*, 91: 102991.
- 613 Cleveland, R., Cleveland, W., McRae, J., Terpenning, I., 1990. STL: A seasonal-trend
614 decomposition procedure based on loess. *Journal of Official Statistics* 6(1): 3-73.
- 615 Deep, K., Thakur, M., 2007a. A new crossover operator for real coded genetic algorithms.
616 *Applied Mathematics and Computation* 188(1), 895-911.
- 617 Deep, K., Thakur, M., 2007b. A new mutation operator for real coded genetic algorithms.
618 *Applied Mathematics and Computation* 193(1), 211-230.
- 619 de Oliveira, D.G.G., Diederichs, M., Thewes, M., 2019b. EPB excavation of cohesive mixed
620 soils: combined methodology for clogging and flow assessment. In: ITA-WTC 2019,
621 Tunnels and Underground Cities: Engineering and Innovation meet Archaeology,
622 Architecture and Art, Naples, Italy, pp. 2008-2017.
- 623 de Oliveira, D.G.G., Diederichs, M., Thewes, M., 2019c. EPB machine excavation of mixed
624 soils – laboratory characterisation. *Geomech. Tunnel. J.* 12 (4): 373-385.

625 de Oliveira, D.G.G., Thewes, M., Diederichs, M., 2019a. Clogging and flow assessment of
626 cohesive soils for EPB tunnelling: Proposed laboratory tests for soil characterisation.
627 *Tunnelling and Underground Space Technology* 94: 103110.

628 de Oliveira, D.G.G., Thewes, M., Diederichs, M.S., & Langmaack, L. (2018). EPB tunnelling
629 through clay-sand mixed soils: Proposed methodology for clogging evaluation.
630 *Geomechanics and Tunnelling* 11(4): 375–387.

631 Feinendegen, M., Ziegler, M., Spagnoli, G., Fernández-Steeger, T., Stanjek, H., 2010. A new
632 laboratory test to evaluate the problem of clogging in mechanical tunnel driving with
633 EPB-shields. In: ISRM International Symposium-eurock, Lausanne, Switzerland, pp.
634 429-432.

635 Feinendegen, M., Ziegler, M., Weh, M., Spagnoli, G., 2011. Clogging during EPB-tunnelling:
636 Occurrence, classification and new manipulation methods. In: Proceedings ITA-AITES
637 World Tunnel Congress, Helsinki, pp. 767-776.

638 Fontaine, E.R., 1954. Investigations into the mechanism of soil adhesion. *European Journal*
639 *of Soil Science* 5(2): 251-263.

640 Gurocak, Z., Solanki, P., Alemdag, S., Zaman, M., 2012. New considerations for empirical
641 estimation of tensile strength of rocks. *Engineering Geology* 145-146, 1-8.

642 Heuser, M., Spagnoli, G., Leroy, P., Klitzsch, N., Stanjek, H., 2012. Electro-osmotic flow in
643 clays and its potential for reducing clogging in mechanical tunnel driving. *Bulletin of*
644 *Engineering Geology and the Environment* 71: 721-733.

645 Hollmann, F.S., Thewes, M., 2013. Assessment method for clay clogging and disintegration
646 of fines in mechanised tunnelling. *Tunnelling and Underground Space Technology* 37:
647 96-105.

648 Hu, W., Rostami, J., 2020. A new method to quantify rheology of conditioned soil for
649 application in EPB TBM tunneling. *Tunnelling and Underground Space Technology* 96:
650 103192.

651 Jia, X., 2004. Theoretical analysis of the adhesion force of soil to solid materials. *Biosystems*
652 *Engineering* 87(4): 489-493.

653 Kang, C., Wu, Y., Yi, Y., Bayat, A., 2019. Assessment of the clogging potential of two clays.
654 *Applied Clay Science* 178: 105134.

655 Kang, C., Yi, Y., Bayat, A., 2018. Performance evaluation of TBM clogging potential for plain
656 and conditioning soil using a newly developed laboratory apparatus. *International*
657 *Journal of Geotechnical Engineering*: 1-10. doi: 10.1080/19386362.2018.1439671

658 Liu, F.T., Ting, K.M., Zhou, Z.H., 2012. Isolation-based anomaly detection. *ACM Transactions*
659 *on Knowledge Discovery from Data* 6(1): 1-39.

660 Masters, T., 1993. Practical neural network recipes in C++. Academic Press, San Diego, CA.

661 Ni, J.C., Cheng, W. (2010). Using fracture grouting to lift structures in clayey sand. *Journal of*
662 *Zhejiang University-SCIENCE A* 11(11): 879-886.

663 Pedregosa, F., Varoquaux, G., Gramfort, A., Michel, V., Thirion, B., Grisel, O., Blondel, M.,
664 Prettenhofer, P., Weiss, R., Dubourg, V. and Vanderplas, J., 2011. Scikit-learn:
665 Machine learning in Python. *Journal of Machine Learning Research* 12: 2825-2830.

666 Pelia, D., Picchio, A., Martinelli, D., Dal Negro, E., 2015. Laboratory tests on soil conditioning
667 of clayey soil. *Acta Geotechnica* 11(5): 1061-1074.

668 Persons, W.M., 1919. Indices of business conditions: An index of general business conditions.
669 Cambridge, MA: Harvard University Press.

670 Rousseeuw, P.J., 1984. Least median of squares regression. *Journal of the American*
671 *Statistical Association* 79(388): 871-880.

672 Ryu, Y.M., Kwon, Y.S., Kim, T.H., Lee, I.M., 2019. Slurry clogging criteria for slurry shield
673 tunnelling in highly permeable ground. *KSCE Journal of Civil Engineering*: 1-10. doi:
674 10.1007/s12205-019-2156-x

675 Sass, I., Burbaum, U., 2008. A method for assessing adhesion of clays to tunneling machines.
676 *Bulletin of Engineering Geology and the Environment* 68(1): 27-34.

677 Schölkopf, B., Platt, J.C., Shawe-Taylor, J., Smola, A.J., Williamson, R. C., 2001. Estimating
678 the support of a high-dimensional distribution. *Neural Computation* 13(7): 1443-1471.

679 Sheil, B., Suryasentana, S.K., Cheng, W.C., 2020. Assessment of anomaly detection methods
680 applied to microtunneling. *Journal of Geotechnical and Geoenvironmental Engineering*,
681 146(9): 04020094.

682 Soomro, M.A., Kumar, M., Xiong, H., Mangnejo, D.A., Mangi, N., 2020. Investigation of effects
683 of different construction sequences on settlement and load transfer mechanism of
684 single pile due to twin stacked tunnelling. *Tunnelling and Underground Space*
685 *Technology* 96: 103171.

686 Spagnoli, G., Feinendegen, M., Seidl, W., 2019b. The impact of mineralogy and chemical
687 conditioning on the mechanical and adhesive properties of clays. In: XVII European
688 Conference on Soil Mechanics and Geotechnical Engineering 2019, Geotechnical
689 Engineering Foundation of the Future, Reykjavik, Iceland.

690 Spagnoli, G., Feinendegen, M., Stanjek, H., Azzam, R., 2011a. Soil conditioning for clays in
691 EPBMs. *Tunnels & Tunnelling International* 43(10): 56-61.

692 Spagnoli, G., Feinendegen, M., Ziegler, M., 2019a. Assessing the clogging potential of
693 clay/additive mixtures by cone pull-out tests. *Geomechanics and Tunnelling* 12(4),
694 362-371.

695 Spagnoli, G., Klitzsch, N., Fernandez-Steeger, T., Feinendegen, M., Rey, A.R., Stanjek, H.,
696 Azzam, R., 2011b. Application of electro-osmosis to reduce the adhesion of clay during
697 mechanical tunnel driving. *Environmental & Engineering Geoscience* 17(4): 417-426.

698 Spagnoli, G., Rubinos, D., Stanjek, H., Fernandez-Steeger, T., Feinendegen, M., Azzam, R.,
699 2012a. Undrained shear strength of clays as modified by pH variations. *Bulletin of*
700 *Engineering Geology and the Environment* 71(1): 135-148.

701 Spagnoli, G., Stanjek, H., Feinendegen, M., Azzam, R., 2014. Mineralogical, mechanical and
702 electrical properties of the clays and their relation with regard to the clogging during
703 mechanical tunnel driving. In: Geo-Congress 2014, Geo-Characterization and
704 Modeling for Sustainability, Atlanta, USA, pp. 495-504.

705 Spagnoli, G., Stanjek, H., Sridharan, A., 2012b. Influence of ethanol/water mixture on the
706 undrained shear strength of pure clays. *Bulletin of Engineering Geology and the*
707 *Environment* 71(2): 389-398.

708 Ong, D.E.L. and Choo, C.S., 2016. Back-analysis and finite element modeling of jacking forces
709 in weathered rocks. *Tunnelling and Underground Space Technology*, 51: 1-10.

710 Tan, Y., Wei, B., 2012. Performance of an overexcavated metro station and facilities nearby.
711 *Journal of Performance of Constructed Facilities*, 26(3): 241-254.

712 Thewes, M., 1999. Adhesion of clay soil in tunnel drives with slurry shields (In German:
713 Adhäsion von Tonböden beim Tunnelvortrieb mit Flüssigkeitsschilden). Berichte aus
714 Bodenmechanik und Grundbau der Bergischen Universität Wuppertal, Fachbereich
715 Bauingenieurwesen, Bd. 21. Shaker Verlag, Aachen.

716 Thewes, M., Burger, W., 2005. Clogging of TBM drives in clay – identification and mitigation
717 of risks. In: Proceedings ITA-AITES World Tunnel Congress, Istanbul, Turkey, pp.
718 737–742.

719 Thewes, M., Hollmann, F.S., 2014. TBM-specific testing scheme to assess the clogging
720 tendency of rock. *Geomechanics and Tunnelling* 7(5): 520-527.

721 Thewes, M., Hollmann, F.S., 2016. Assessment of clay soils and clay-rich rock for clogging of
722 TBMs. *Tunnelling and Underground Space Technology* 57: 122-128.

723 Tombacz, E., Szekeres, M., 2006. Surface charge heterogeneity of kaolinite in aqueous
724 suspension in comparison with montmorillonite. *Applied Clay Science* 34: 105-124.

725 van Baalen, L.R., 1999. Reduction of clay adherence by electroosmosis. Master thesis,
726 Faculty of Civil Engineering and Geosciences, TU Delft.

727 van Baalen, L.R., Zimnik, A., Verhoef, P., Ngan-Tillard, D., 2001. Applicability of electro-
728 osmosis to reduce clay adhesion in a TBM. In Proceedings of the International
729 Conference on Geotechnical Geological Engineering. Melbourne.

730 Vapnik, V., 1995. The nature of statistical learning theory. Springer, New York.

731 Yin, Z.Y., Jin, Y.F., Huang, H.W., Shen, S.L., 2016. Evolutionary polynomial regression based
732 modelling of clay compressibility using an enhanced hybrid real-coded genetic
733 algorithm. *Engineering Geology* 210, 158-167.

734 Zhang, F., Kong, R., Peng, J., 2018. Effects of heating on compositional, structural, and
735 physicochemical properties of loess under laboratory conditions. *Applied Clay Science*
736 152: 259-266.

737 Zhang, W.G., Li, H.R., Wu, C.Z., Li, Y.Q., Liu, Z.Q., Liu, H.L., 2020b. Soft computing approach
738 for prediction of surface settlement induced by earth pressure balance shield tunneling.
739 *Underground Space*, in Press. doi: 10.1016/j.undsp.2019.12.003

740

741 Zhang, C., Yang, J., Fu, J., Wang, S., Yin, J., & Xie, Y., 2020a. Recycling of discharged soil
742 from EPB shield tunnels as a sustainable raw material for synchronous grouting.
743 *Journal of Cleaner Production* 268: 121947.

744 Zhang, W.G., Zhang, R., Wu, C., Goh, A.T.C., Lacasse, S., Liu, Z., Liu, H., 2020c. State-of-
745 the-art review of soft computing applications in underground excavations. *Geoscience*
746 *Frontiers* 11(4): 1095-1106. doi: 10.1016/j.gsf.2019.12.003

747 Zumsteg, R., Plötze, M., Puzrin, A., 2013. Reduction of the clogging potential of clays: new
748 chemical applications and novel quantification approaches. *Geotechnique* 63(4): 276-
749 286.

750 Zumsteg, R., Puzrin, A.M., Anagnostou, G., 2016. Effects of slurry on stickiness of excavated
751 clays and clogging of equipment in fluid supported excavations. *Tunnelling and*
752 *Underground Space Technology* 58: 197-208.

753

754 List of figures

Fig. 1 Illustration of one-class support vector machine approach and the construction of the hyperplane by transforming the original input space into a high-dimensional feature space

Fig. 2 Illustration of isolation forest approach and the construction of separate isolation trees by randomly sampling from the training dataset. Red circles represent outliers, blue circles indicate uncommon inliers and light blue circles represent common inliers

Fig. 3 Illustration of robust covariance approach showing the use of a robust estimator of covariance to reflect the true organisation of observations using the Mahalanobis distance

Fig. 4 Pipejacking project description: (a) location of the four drives in Taipei, Taiwan and (b) geological profile derived from four nearby boreholes

Fig. 5 Soil properties profile

Fig. 6 Grain-size distribution curves for drives B, C and D

Fig. 7 Monitored data for drive B: (a) development of jacking force, jacking speed and cutterwheel torque with jacking distance and (b) development of density of support slurry with jacking distance

Fig. 8 Monitored data for drive C: (a) development of jacking force, jacking speed and cutterwheel torque with jacking distance and (b) development of density of support slurry with jacking distance

Fig. 9 Monitored data for drive D: (a) development of jacking force, jacking speed and cutterwheel torque with jacking distance and (b) development of density of support slurry with jacking distance

Fig. 10 Universal classification diagram for the assessment of anomalous clogging behaviour

Fig. 11 Performance of AD approaches applied to drive B using transformed slurry density space: (a) OCSVM, (b) Robcov and (c) IForest

Fig. 12 Performance of AD approaches applied to drive D using transformed slurry density space: (a) OCSVM, (b) Robcov and (c) IForest

Fig. 13 Performance of AD approaches applied to drive B using transformed maximum torque space: (a) OCSVM, (b) Robcov and (c) IForest

Fig. 14 Performance of AD approaches applied to drive D using transformed maximum torque space: (a) OCSVM, (b) Robcov and (c) IForest

Fig. 15 Performance of AD approaches applied to drive B using transformed jacking speed space: (a) OCSVM, (b) Robcov and (c) IForest

Fig. 16 Performance of AD approaches applied to drive D using transformed jacking speed space: (a) OCSVM, (b) Robcov and (c) IForest

Fig. 17 Simple diagram for TBM operator to assess tendency to clayey clogging during slurry-supported pipejacking

Fig. 18 Clayey clogging with embedded gravel occurred while spanning through a ground composed of the clayey gravel and the gravel at drive B: (a) before and (b) after the clay soil adhered to cutterwheel

Fig. 19 Real-time anomaly detection scheme for tunnel construction in clayey soil

756 List of tables

Table 1 Summary of geological data and shield machine performance data

Table 2 Summary of residual and trend components of datapoints and their behaviour relevant to anomalous behaviour formation

Table 3 Summary of discovery rate and false alarm rate

757

758

Table 1 Summary of geological data and shield machine performance data

Geological data										Performance data of TBM or slurry-supported shield			
Data source	Particle distribution			Unit weight (kN/m ³)	Natural water content (%)	Atterberg limits			Consistency I_c	USCS symbol	Cutterwheel torque T_c (Amp or kN·m)	Thrust force F_T (kN)	Jacking speed V (r/min)
	Sand	FC	Clay			LL (%)	PL (%)	PI (%)					
Tokgöz (2016)	-	84.0	3.9	17.4	36.0	70	28	42	0.81	CH	70	350	2.8
	-	88.5	4.6	16.8	39.5	65	25	40	0.64	CH			
	-	89.3	6.5	16.8	31.0	88	30	58	0.98	CH	90	255	2.8
	-	92.6	6.5	17.9	33.8	90	30	60	0.94	CH			
	-	99.8	7.7	17.6	39.0	91	36	55	0.95	CH	85	270	2.8
	-	92.7	3.4	18.3	35.1	72	27	45	0.82	CH			
	-	97.5	6.1	17.9	30.0	80	22	58	0.86	CH	87.5	260	2.8
	-	94.5	3.6	17.3	30.2	86	24	62	0.90	CH			
	-	91.0	7.2	17.8	29.4	92	24	68	0.92	CH	87.5	225	2.8
	-	96.6	4.9	17.9	32.3	94	28	56	1.10	CH			
	-	89.8	5.0	17.5	35.0	82	30	52	0.90	CH	75	155	2.8
	-	96.5	6.0	18.0	44.1	81	33	48	0.77	CH			
-	89.8	7.1	17.7	28.5	86	23	63	0.91	CH	80	250	2.8	
Woo and Moh (1990)	67.0	33.0	-	19.7	27.7	34	22	12	0.53	CL	-	-	-
	25.0	75.0	-	18.8	29.6	36	23	13	0.49	CL	-	-	-
	34.0	31.0	26.0	16.5	26.6	33.3	22.1	11.2	0.60	CL	-	-	-
	22.0	43.0	26.0	16.7	30.6	26.9	18.6	8.3	-	CL	-	-	-
	-	-	-	14.8	28.5	31.2	22.8	8.4	0.32	CL	-	-	-

Table 1 Summary of geological data and shield machine performance data (cont'd)

Geological data											Performance data of TBM or slurry-supported shield		
Data source	Particle distribution			Unit weight (kN/m ³)	Natural water content (%)	Atterberg limits			Consistency I_c	USCS symbol	Cutterwheel torque T_c (Amp or kN·m)	Thrust force F_T (kN)	Jacking speed V (r/min)
	Sand	FC	Clay			LL (%)	PL (%)	PI (%)					
This study	85.0	14.0	8.0	20.1	22.4	25	15	10	0.26	SC	50	2254	25
	20.5	5.5	1.5	19.1	22.4	28	17	11	0.51	GP-GC	45	2793	80
Avunduk and Copur (2018)	31	69	-	-	30.0	41	19	22	0.49	CL	797 ± 122	4539 ± 562	-
	35	65	-	-	30.0	46	18	28	0.58	CL			
	38	62	-	-	30.0	48	24	24	0.75	CL			
	39	61	-	-	30.0	56	26	30	0.86	CH			
	42	58	-	-	30.0	57	27	30	0.88	CH			
	39	61	-	-	30.0	58	27	31	0.91	CH			
	21	79	-	-	25.0	37	11	26	0.46	CL	517 ± 153	5705 ± 702	-
	68	32	-	-	25.0	-	-	-	-	SM			
	63	37	-	-	25.0	-	-	-	-	SM			
	57	53	-	-	28.0	33	15	19	0.28	CL	475 ± 189	5750 ± 785	-
	49	51	-	-	28.0	33	12	21	0.23	CL			
	30	70	-	-	28.0	35	13	21	0.31	CL			
	27	73	-	-	28.0	40	15	25	0.47	CL			
24	76	-	-	28.0	41	14	26	0.48	CL				
Avunduk and Copur (2019)	67	33	-	-	12.5	49	35.6	13.4	2.72	SC	233	1900	3.6

Table 2 Summary of residual and trend components of datapoints and their behaviour relevant to anomalous behaviour formation

Pipejacking drive	Parameter considered	Datapoint	Residual component R_t	Trend component T_t	Behaviour	Quadrant distribution
B	Density	21	1.00	1.00	1	II
		31	0	0.66	2	I
		41	0.46	0	1	III
	Torque	10	1.00	0.71	1	II
		24	0.77	1.00	1	II
		54	0	0.86	2	I
		90	0.01	0.29	2	III
		110	0.44	0	1	III
		111	0.50	0	1	III
		118	0.34	0	1	III
	Speed	119	0.44	0	1	III
		6	1.00	0.59	2	II
		11	0	0.61	2	I
		23	0.39	0.04	1	III
		24	0.37	0	1	III
		25	0.61	0.16	1	IV
		35	0.98	1.00	1	II
		36	0.20	0.87	2	I
49	0.97	0.84	2	II		

Table 2 Summary of residual and trend components of datapoints and their behaviour relevant to anomalous behaviour formation (cont'd)

Pipejacking drive	Parameter considered	Datapoint	Residual component R_t	Trend component T_t	Behaviour	Quadrant distribution
D	Density	38	0.94	0.42	2	IV
		65	0.87	1.00	1	II
		75	0	0.12	2	III
		79	1.00	0.17	2	IV
	Torque	19	0.62	0.80	2	I
		26	0.38	1.00	1	I
		37	0.43	1.00	1	I
		38	0.65	1.00	1	II
		72	0.19	0	1	III
		73	0.81	0	2	IV
		89	1.00	0.40	2	IV
	Speed	39	0.13	0.16	2	III
		57	0.02	0	1	III
		62	0.88	0.87	1	II
		67	0.21	0.12	1	III
		68	0.22	0.07	1	III
		75	0.06	0.76	2	I
		81	1.00	1.00	1	II
		82	0.88	0.96	1	II
	83	0	0.66	2	I	

Note: density = density of support slurry; torque = cutterwheel torque; speed = jacking speed; I = distribution quadrant of datapoint as per their values of R_t and T_t ; details relevant to behaviours '1' and '2' refer to the beginning of the 'Discussion' section in the main text.

Table 3 Summary of discovery rate and false alarm rate

AD approach	Pipejacking drive	Parameter considered	Number of datapoint	Number of TP	Number of TN	Number of FP	Number of FN	Discovery rate, DR (%)	False alarm rate, FAR (%)
OCSVM	B	Density	29	1	26	2	0	100	7.1
		Torque	58	1	52	5	0	100	8.8
		Speed	60	1	55	4	0	100	6.8
	D	Density	25	0	21	3	1	0	12.5
		Torque	39	1	35	3	0	100	7.9
		Speed	69	1	62	6	0	100	8.8
Robcov	B	Density	29	1	28	0	0	100	0
		Torque	58	0	51	6	1	0	10.5
		Speed	60	1	55	4	0	100	6.8
	D	Density	25	1	22	2	0	100	8.3
		Torque	39	1	35	3	0	100	7.9
		Speed	69	1	62	6	0	100	8.8
IForest	B	Density	29	1	28	0	0	100	0
		Torque	58	1	53	4	0	100	7.0
		Speed	60	1	56	3	0	100	5.1
	D	Density	25	1	23	1	0	100	4.2
		Torque	39	0	34	4	1	0	10.5
		Speed	69	0	62	6	1	0	8.8

Note: density = density of support slurry; torque = cutterwheel torque; speed = jacking speed; TP = true positive; TN = true negative; FP = false positive; FN = false negative.

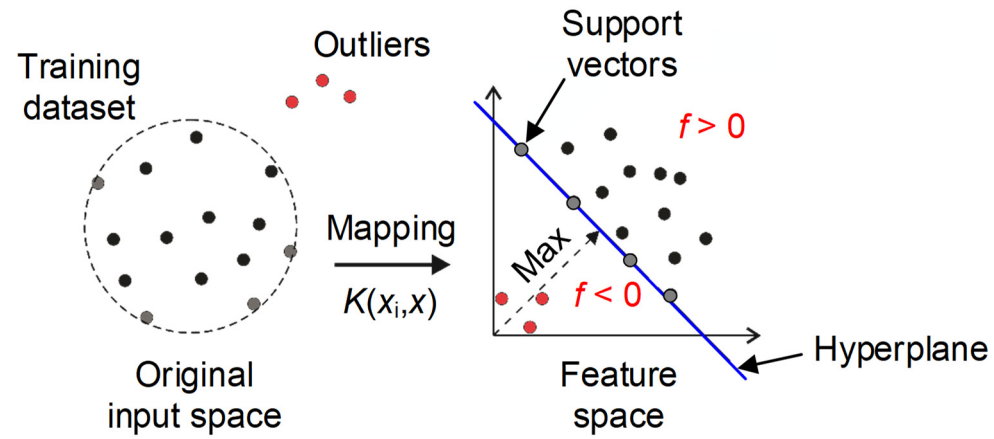


Fig. 1 Illustration of one-class support vector machine approach and the construction of the hyperplane by transforming the original input space into a high-dimensional feature space

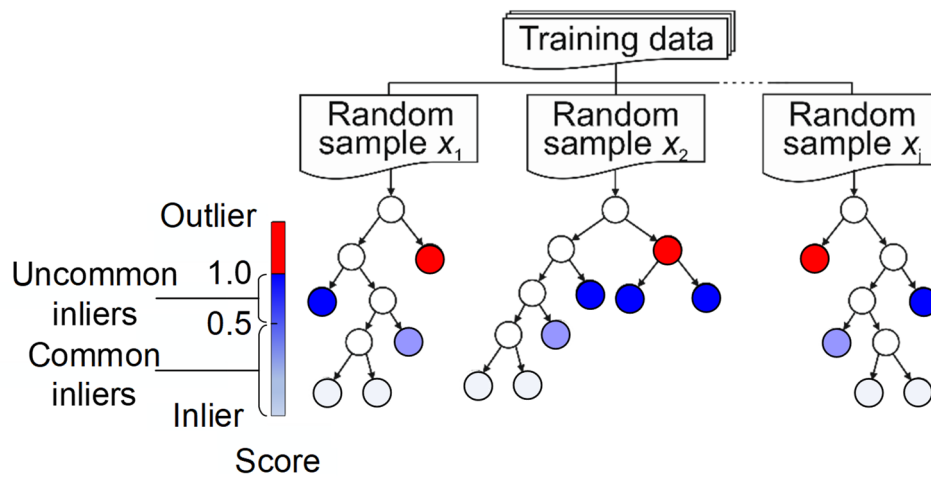


Fig. 2 Illustration of isolation forest approach and the construction of separate isolation trees by randomly sampling from the training dataset. Red circles represent outliers, blue circles indicate uncommon inliers and light blue circles represent common inliers.

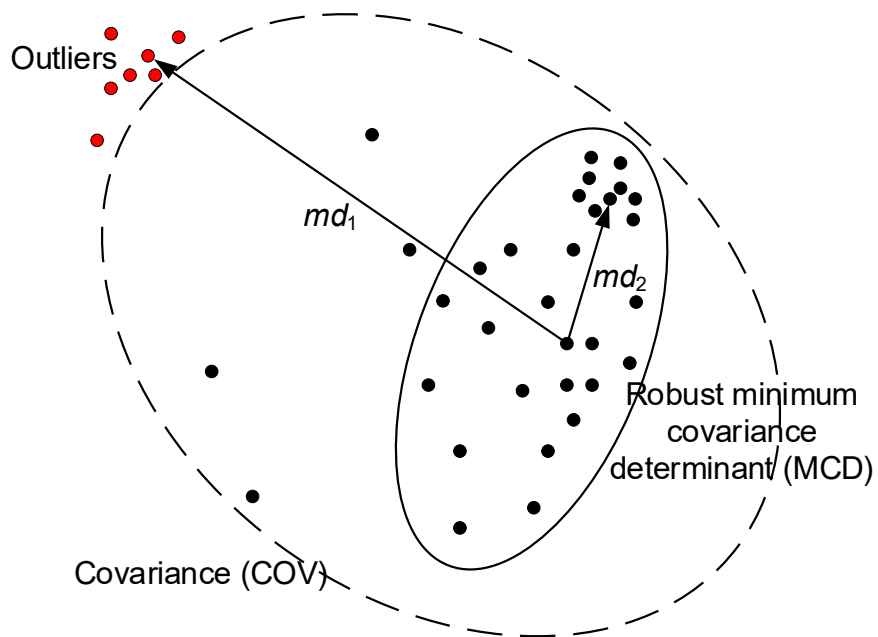
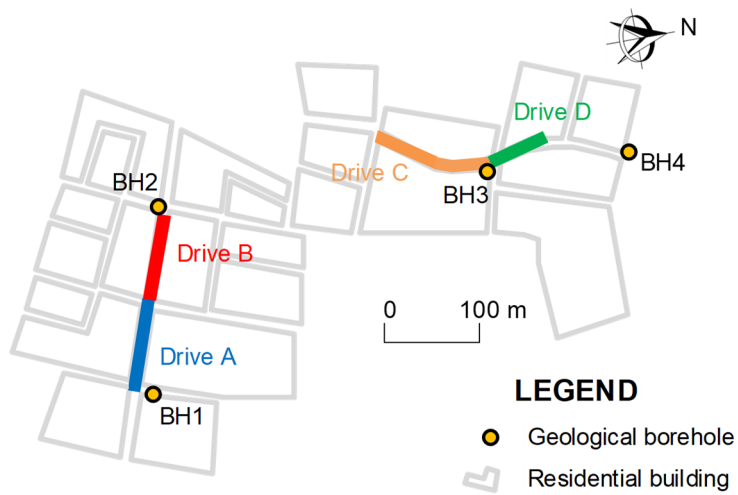
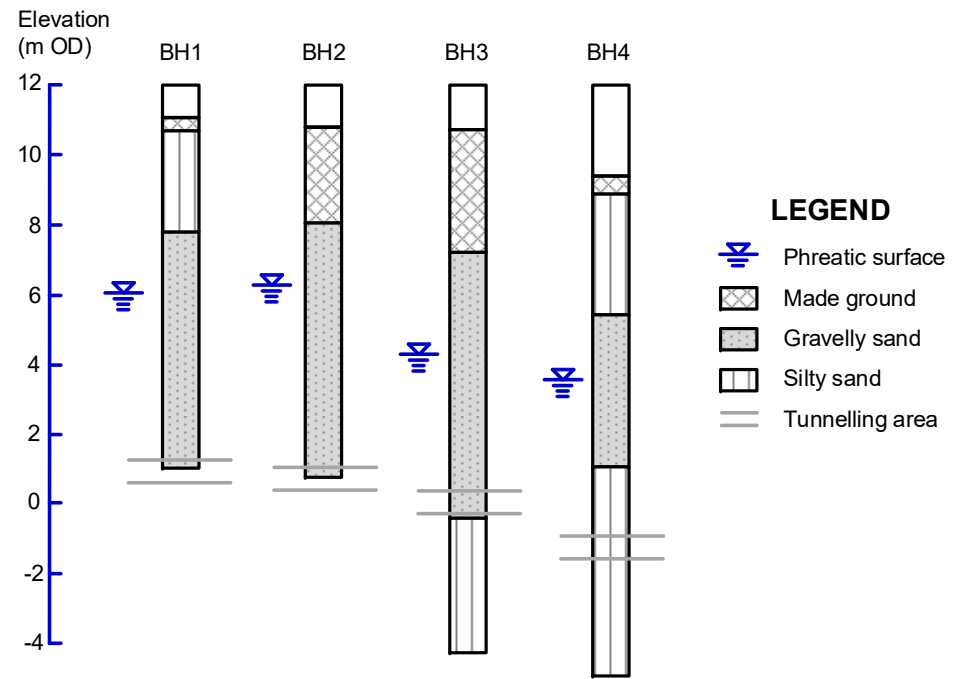


Fig. 3 Illustration of robust covariance approach showing the use of a robust estimator of covariance to reflect the true organisation of observations using the Mahalanobis distance

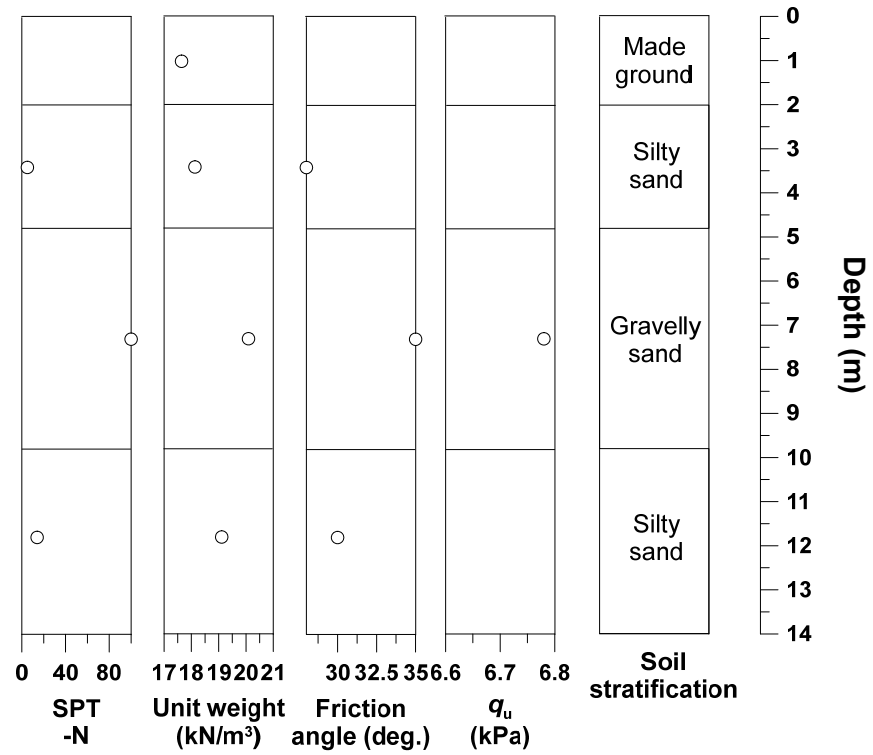


(a)



(b)

Fig. 4 Pipejacking project description: (a) location of four drives in Taipei, Taiwan and (b) geological profile derived from four nearby boreholes



Note: q_u =Unconfined compressive strength; SPT-N=Blow count N value

Fig. 5 Soil properties profile

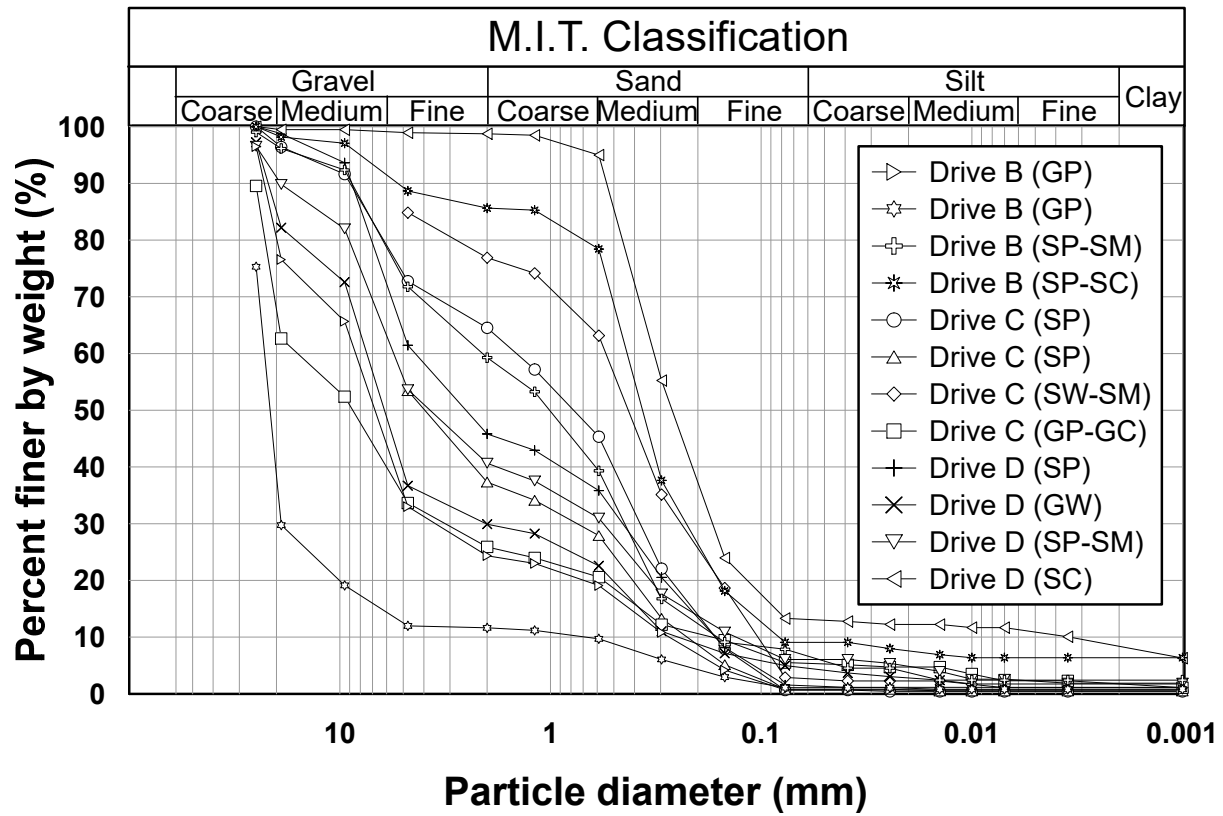
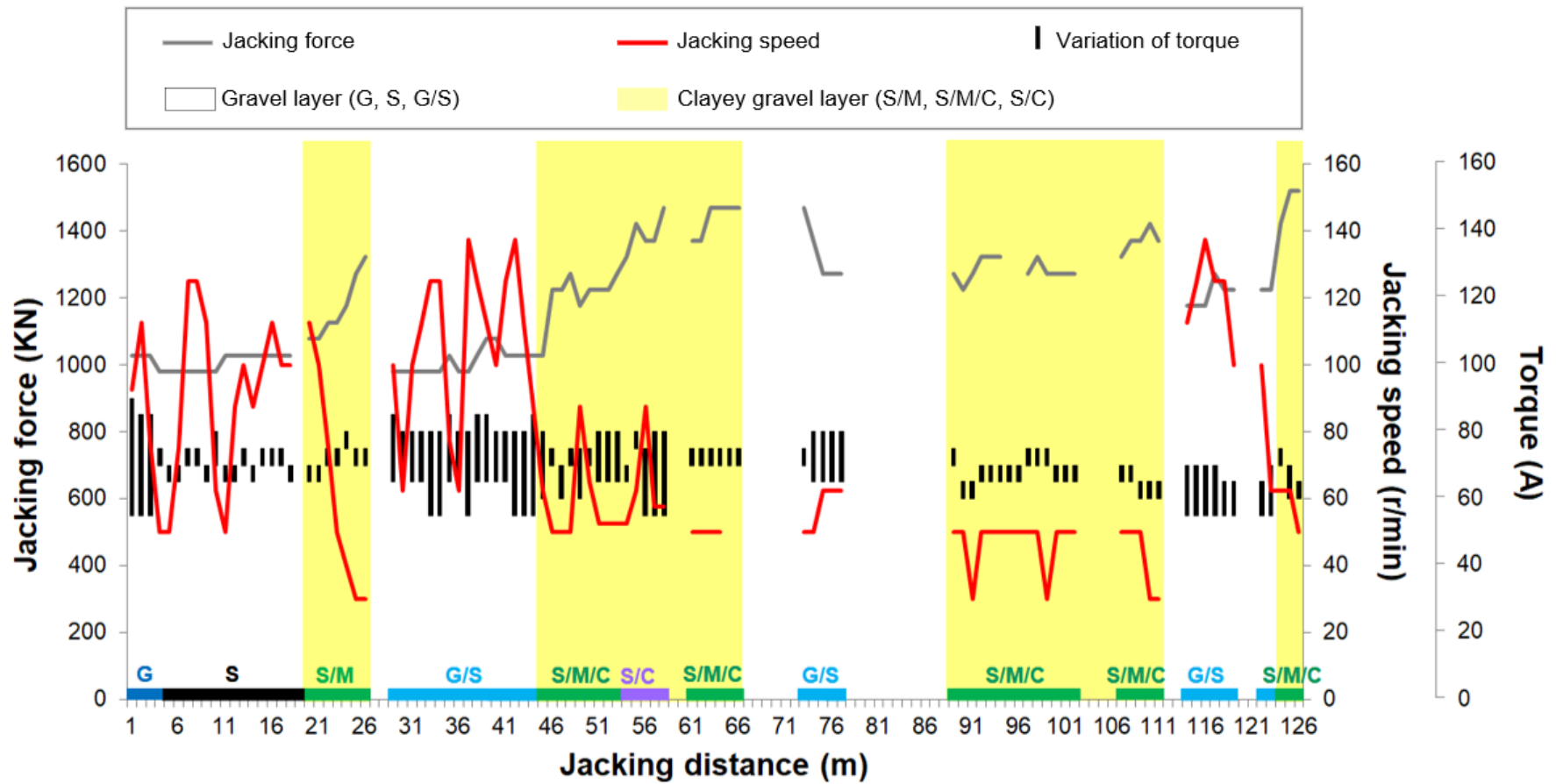
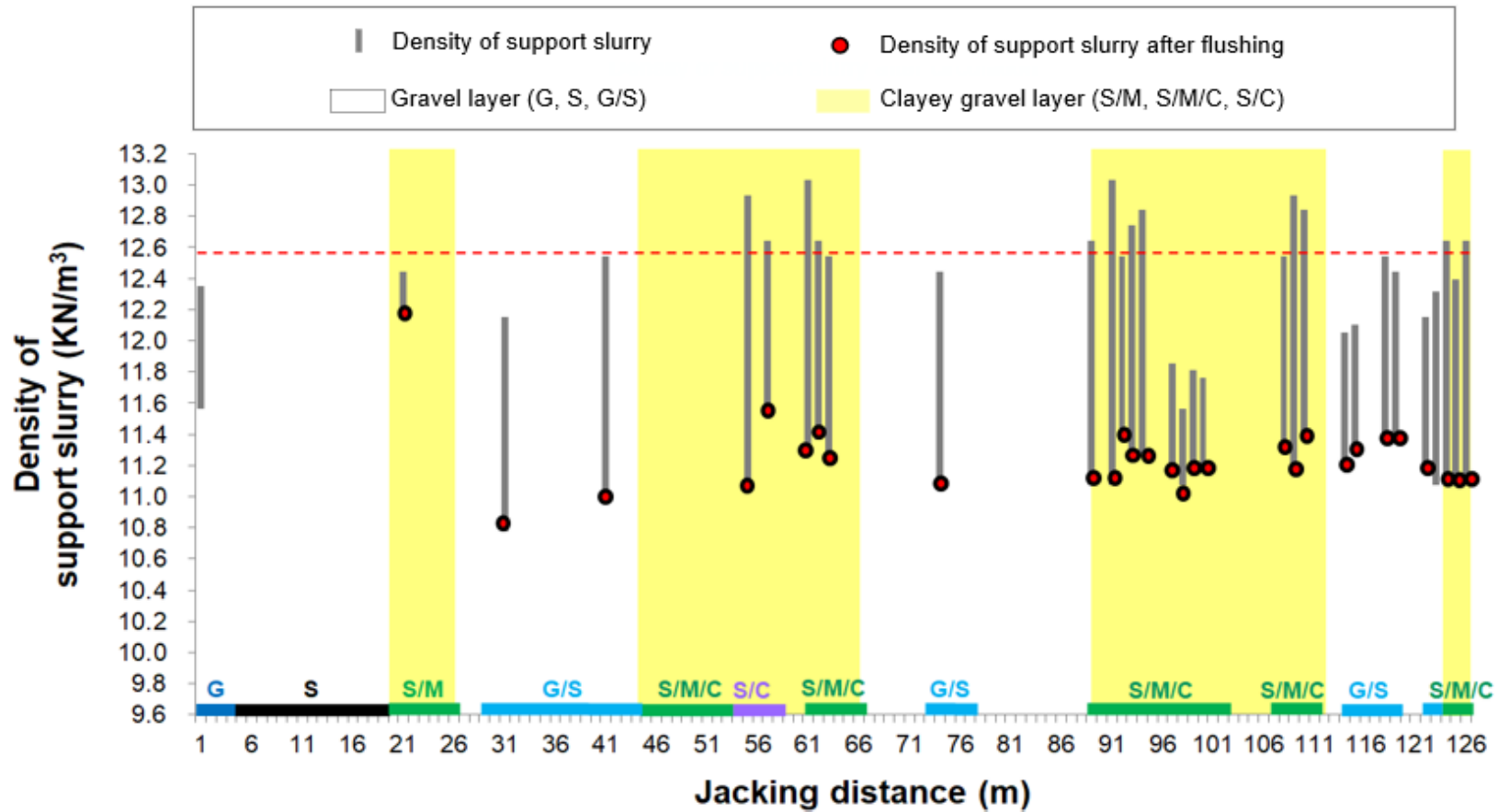


Fig. 6 Grain-size distribution curves for drives B, C and D



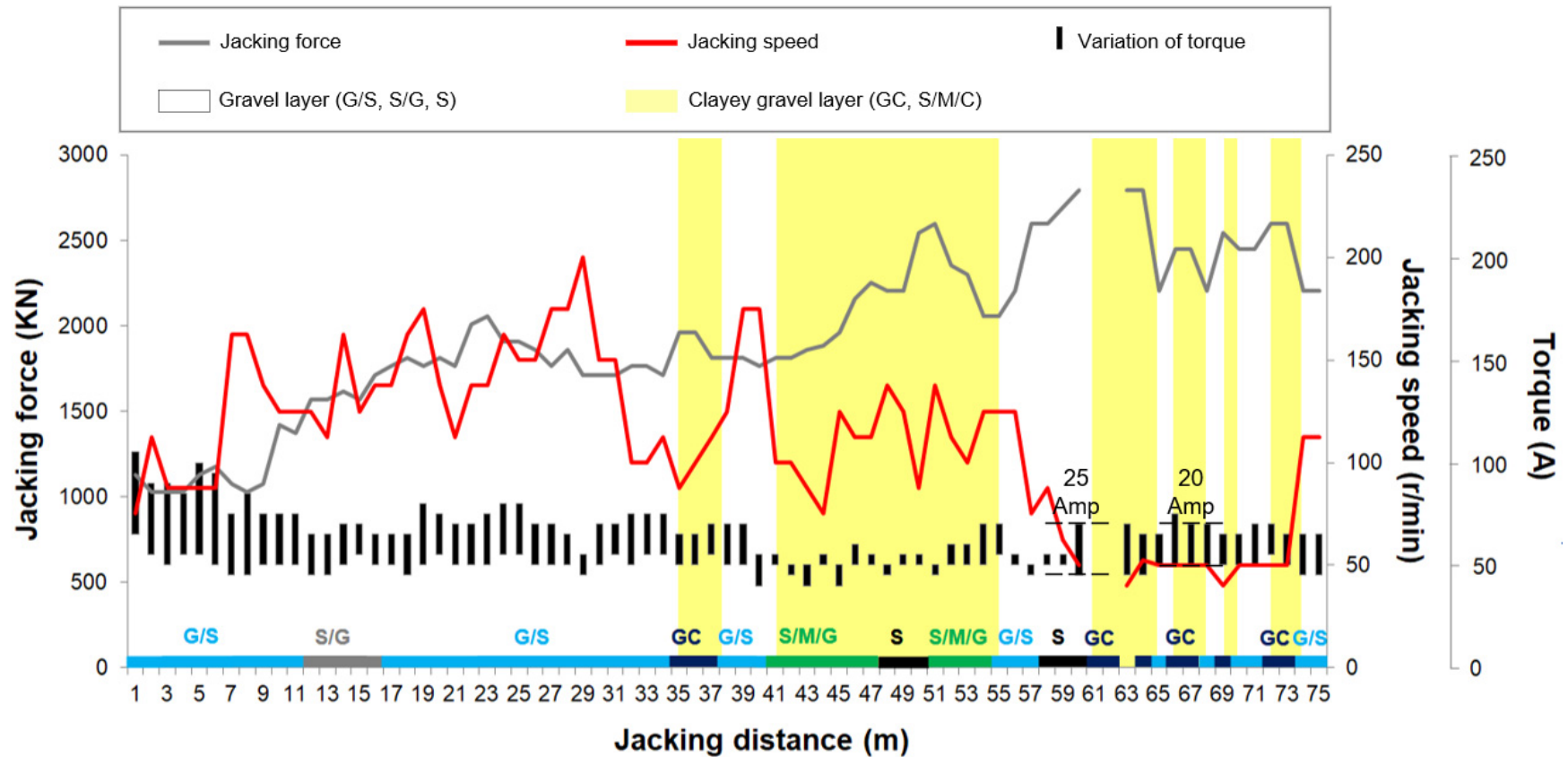
(a)

Fig. 7 Monitored data for drive B: (a) development of jacking force, jacking speed and cutterwheel torque with jacking distance and (b) development of density of support slurry with jacking distance



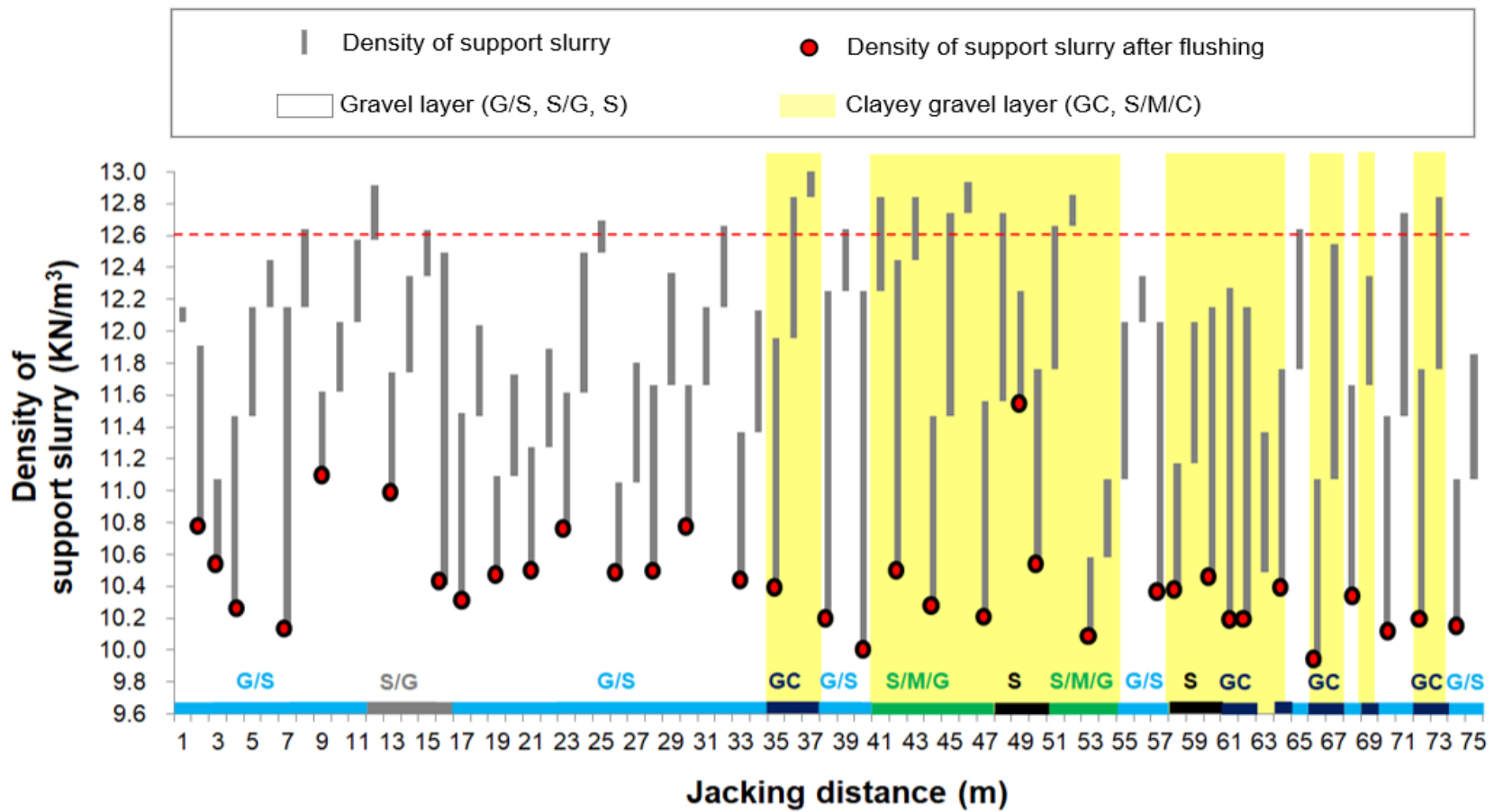
(b)

Fig. 7 Monitored data for drive B: (a) development of jacking force, jacking speed and cutterwheel torque with jacking distance and (b) development of density of support slurry with jacking distance (cont'd)



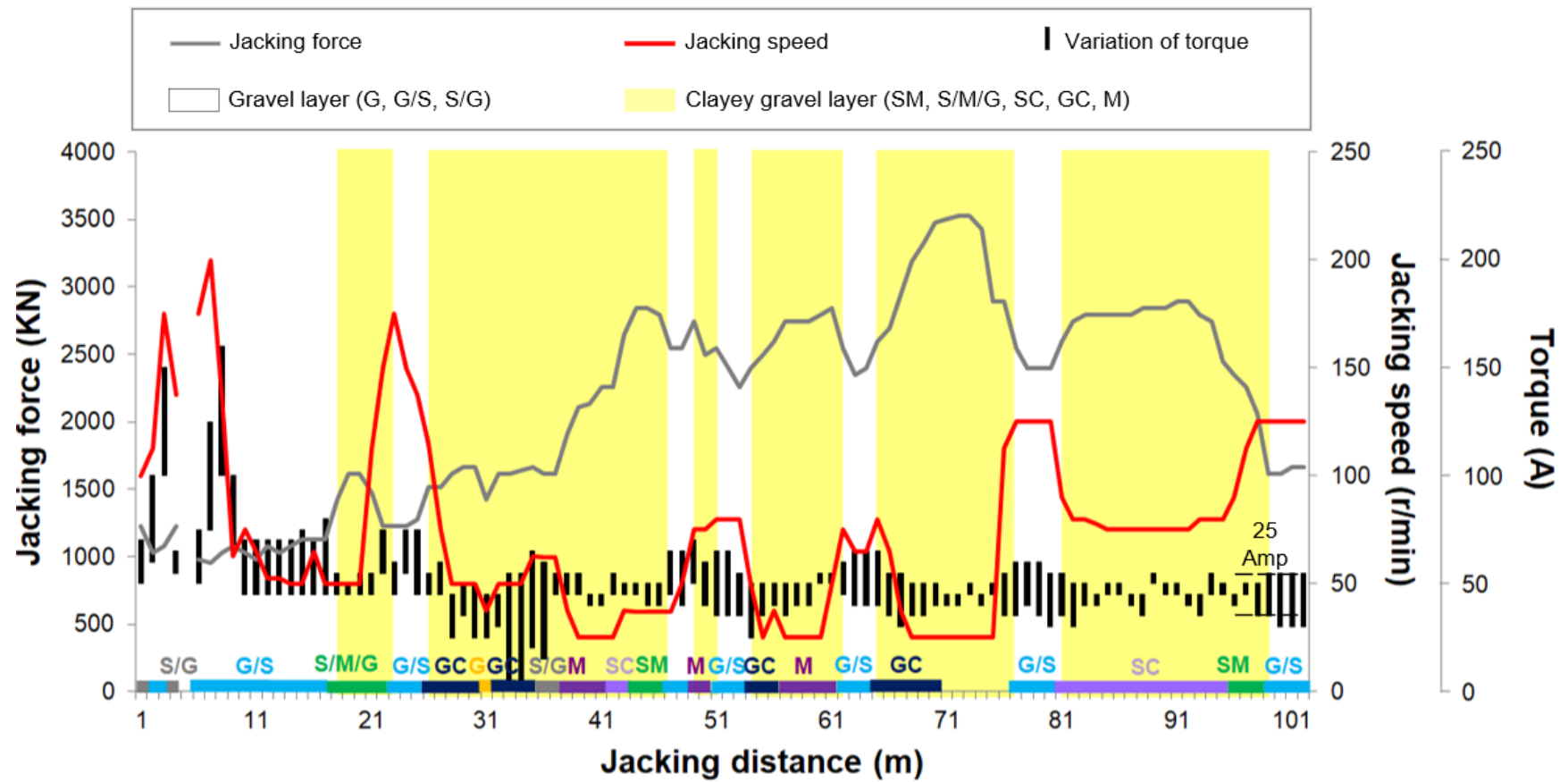
(a)

Fig. 8 Monitored data for drive C: (a) development of jacking force, jacking speed and cutterwheel torque with jacking distance and (b) development of density of support slurry with jacking distance



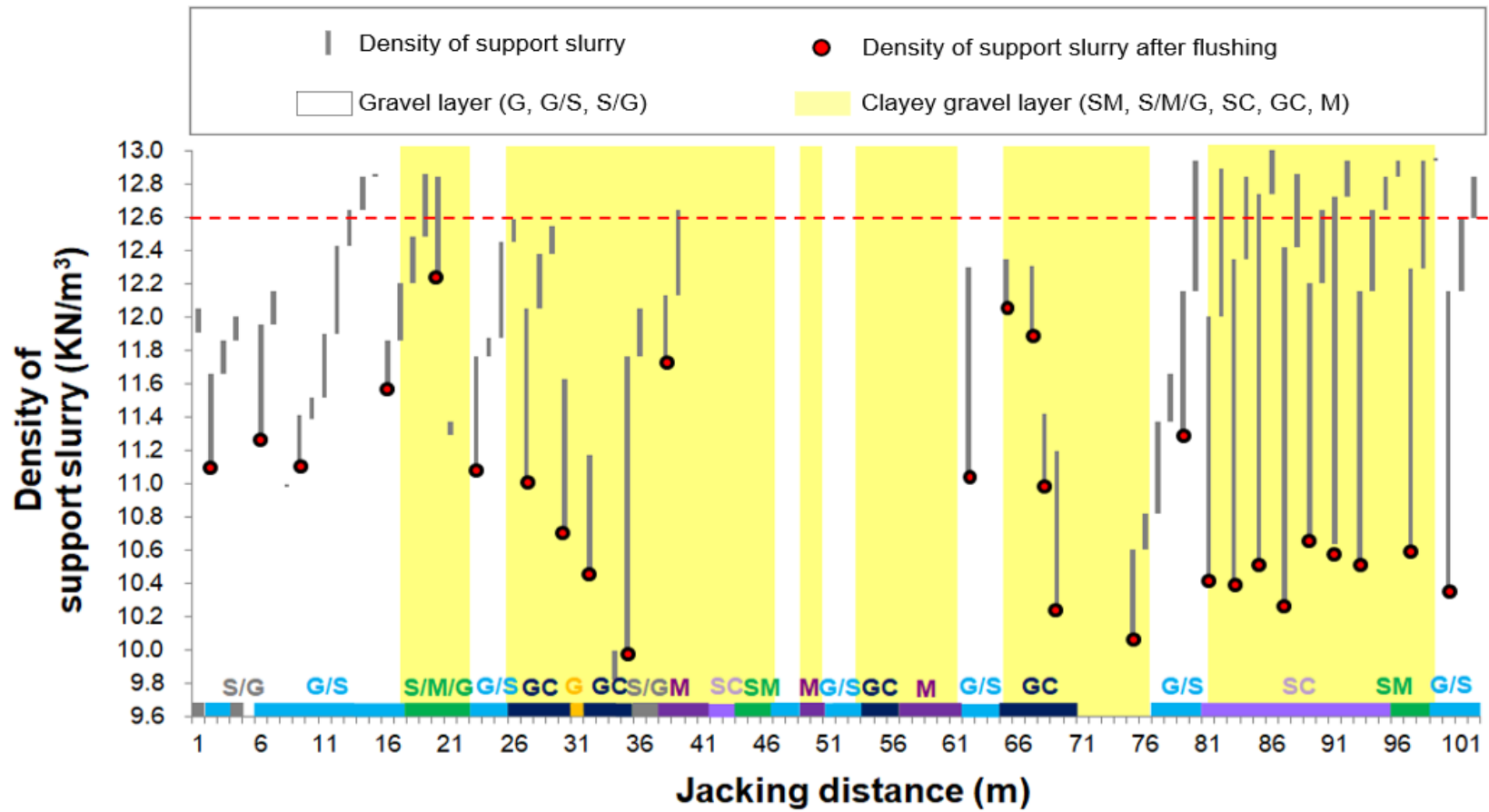
(b)

Fig. 8 Monitored data for drive C: (a) development of jacking force, jacking speed and cutterwheel torque with jacking distance and (b) development of density of support slurry with jacking distance (cont'd)



(a)

Fig. 9 Monitored data for drive D: (a) development of jacking force, jacking speed and cutterwheel torque with jacking distance and (b) development of density of support slurry with jacking distance



(b)

Fig. 9 Monitored data for drive D: (a) development of jacking force, jacking speed and cutterwheel torque with jacking distance and (b) development of density of support slurry with jacking distance (cont'd)

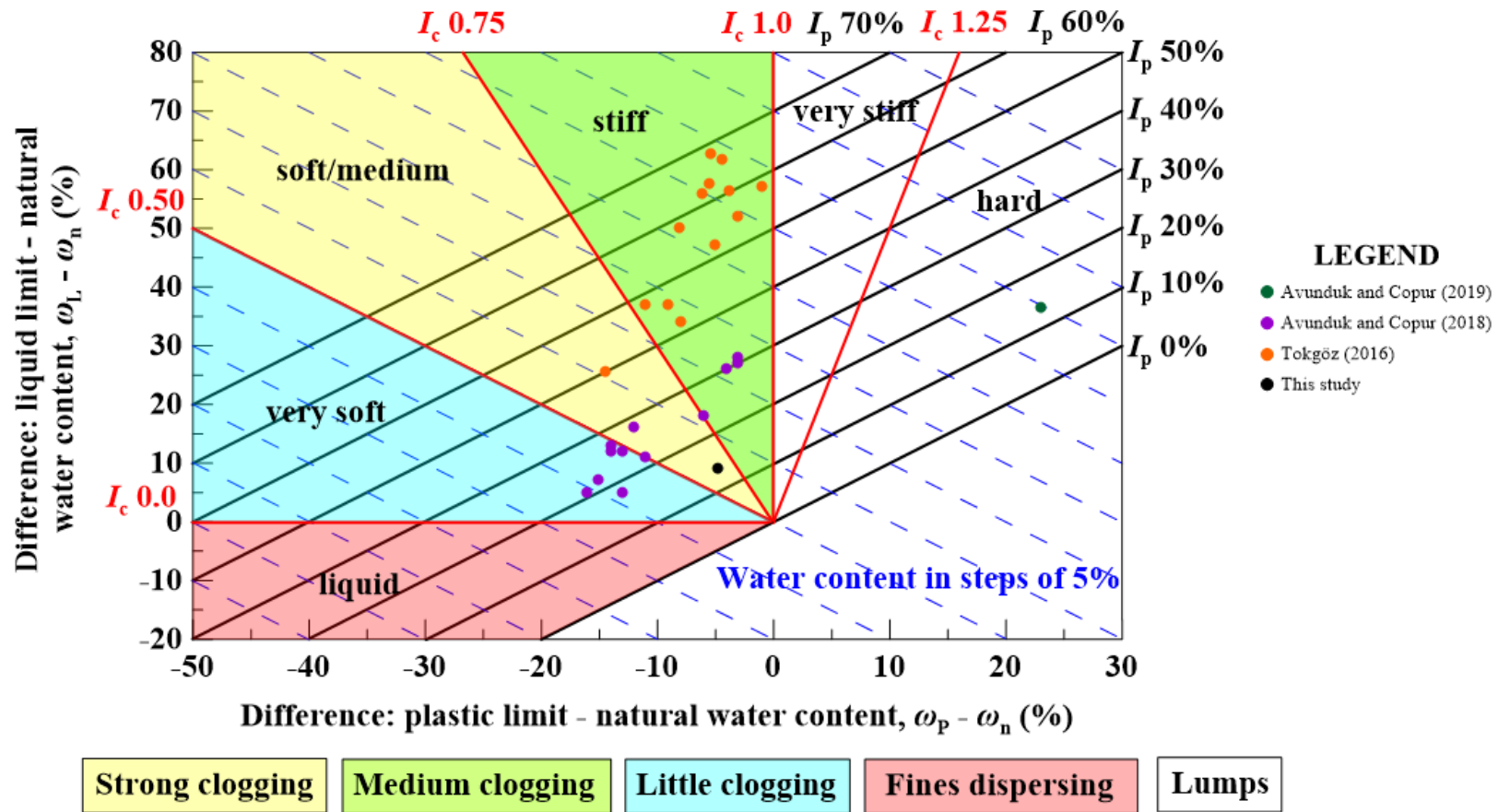
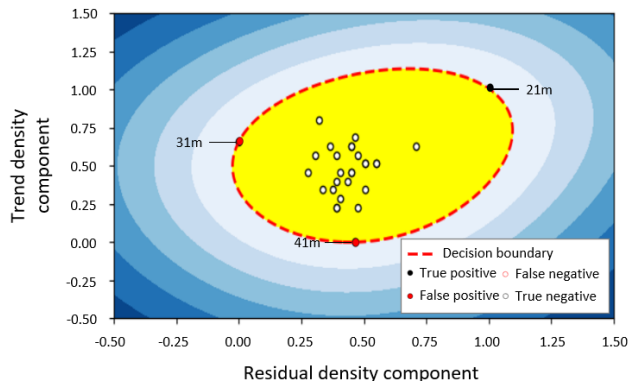
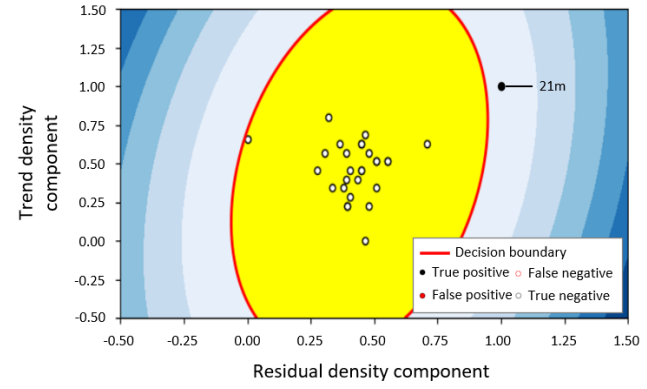


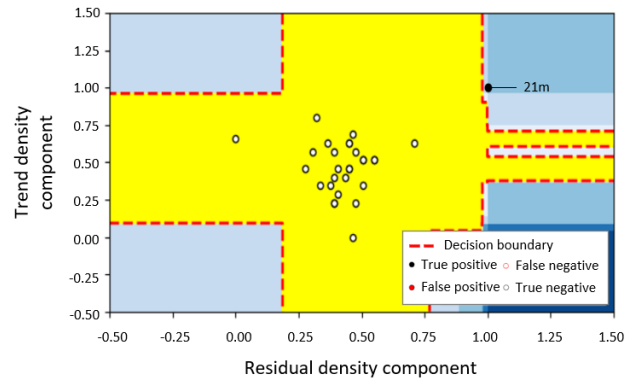
Fig. 10 Universal classification diagram for the assessment of anomalous clogging behaviour



(a)

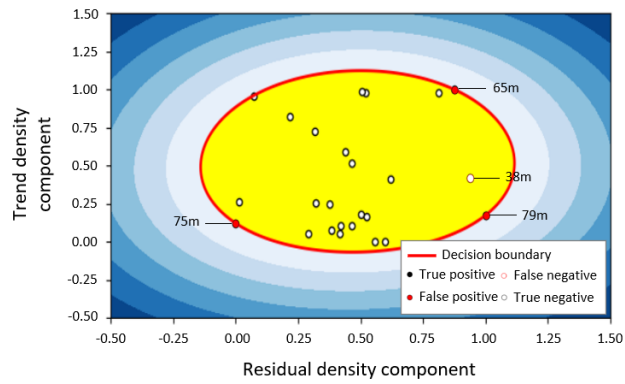


(b)

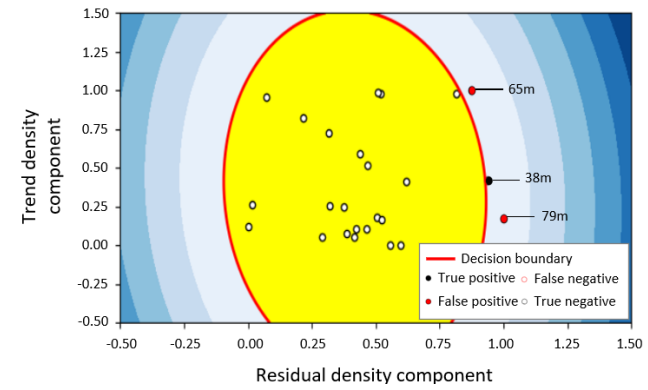


(c)

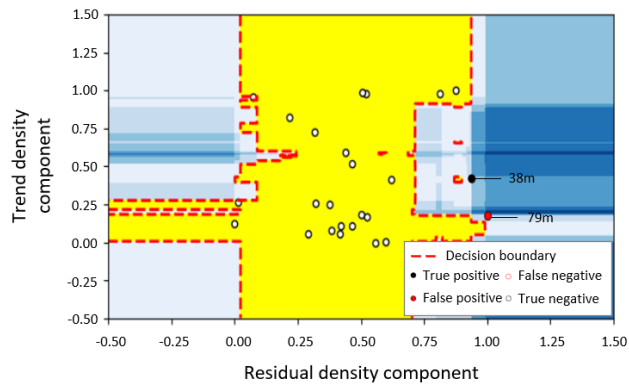
Fig. 11 Performance of AD approaches applied to drive B using transformed slurry density space: (a) OCSVM, (b) Robcov and (c) IForest



(a)

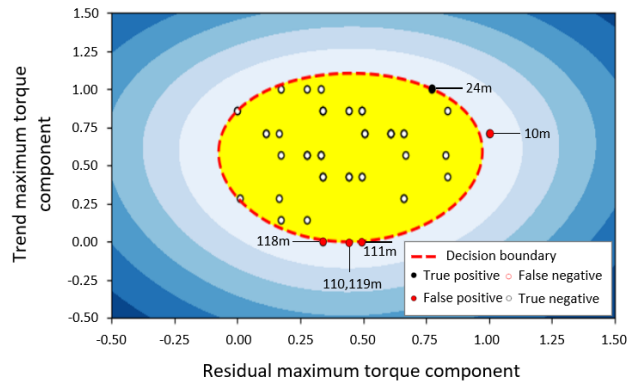


(b)

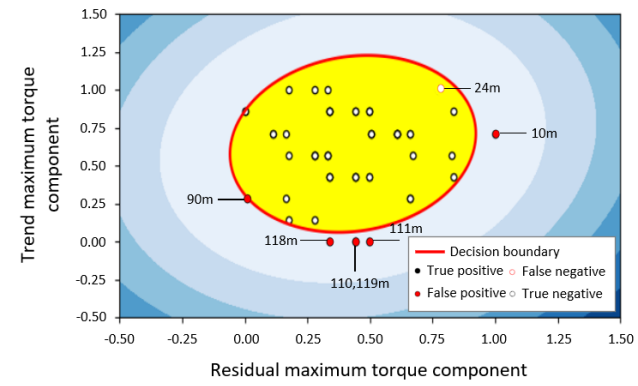


(c)

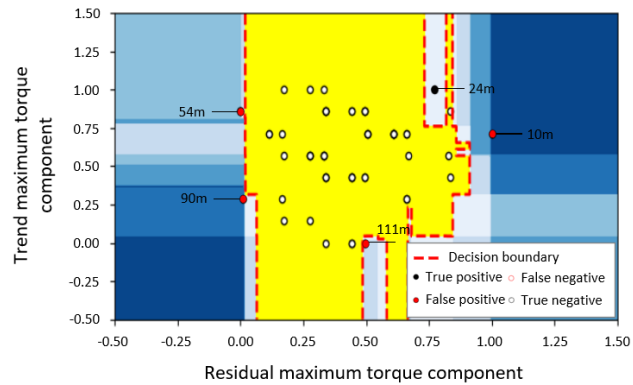
Fig. 12 Performance of AD approaches applied to drive D using transformed slurry density space: (a) OCSVM, (b) Robcov and (c) IForest



(a)

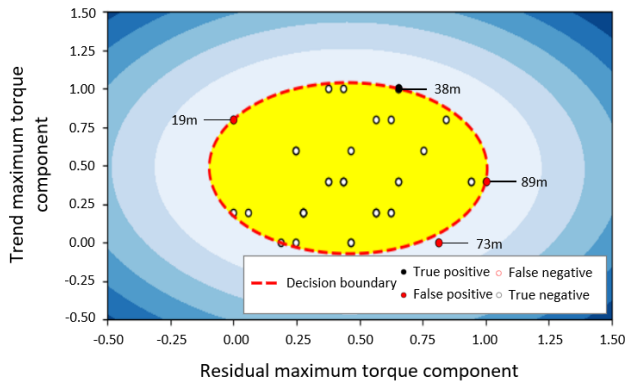


(b)

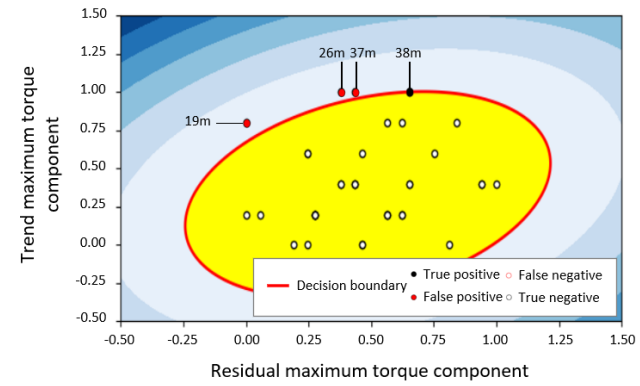


(c)

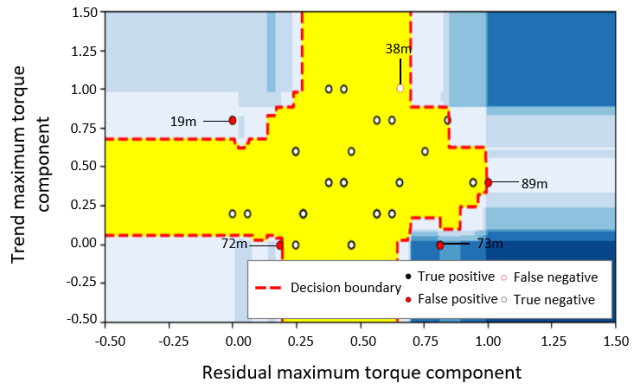
Fig. 13 Performance of AD approaches applied to drive B using transformed maximum torque space: (a) OCSVM, (b) Robcov and (c) IForest



(a)

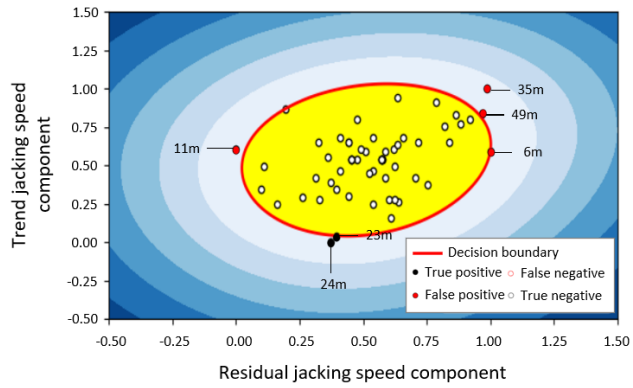


(b)

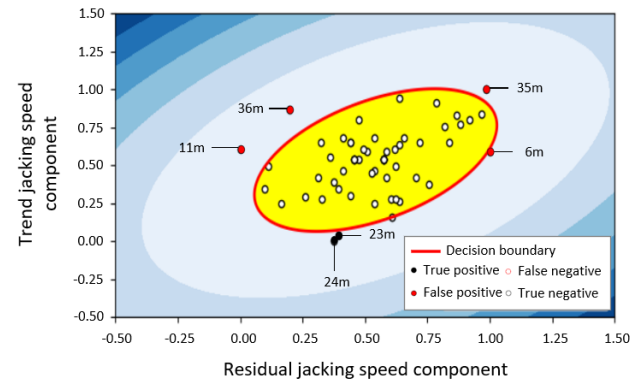


(c)

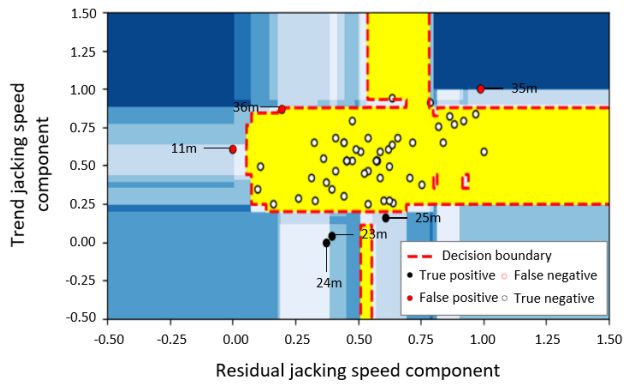
Fig. 14 Performance of AD approaches applied to drive D using transformed maximum torque space: (a) OCSVM, (b) Robcov and (c) IForest



(a)

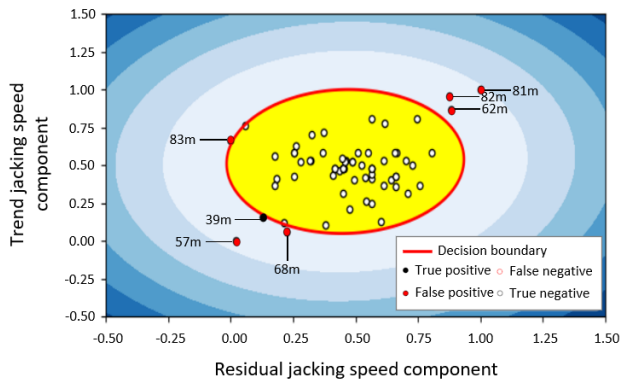


(b)

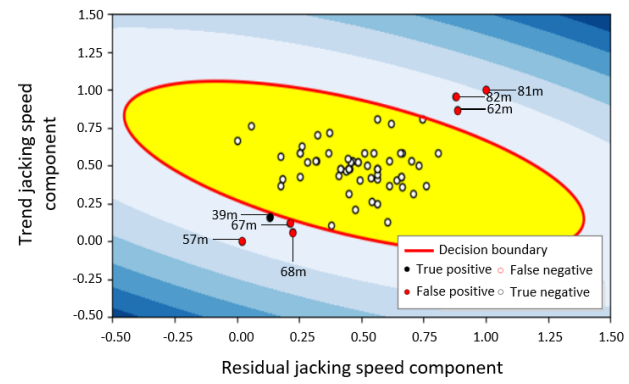


(c)

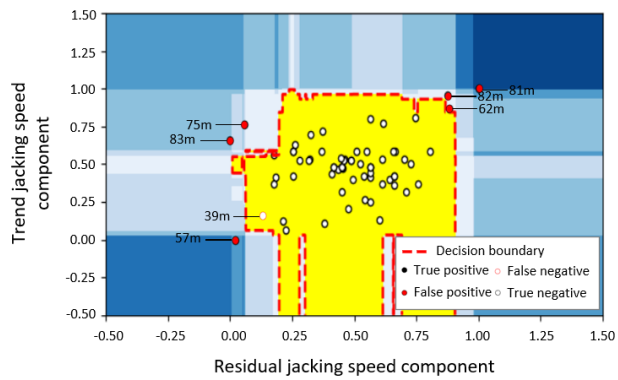
Fig. 15 Performance of AD approaches applied to drive B using transformed jacking speed space: (a) OCSVM, (b) Robcov and (c) IForest



(a)



(b)



(c)

Fig. 16 Performance of AD approaches applied to drive D using transformed jacking speed space: (a) OCSVM, (b) Robcov and (c) IForest

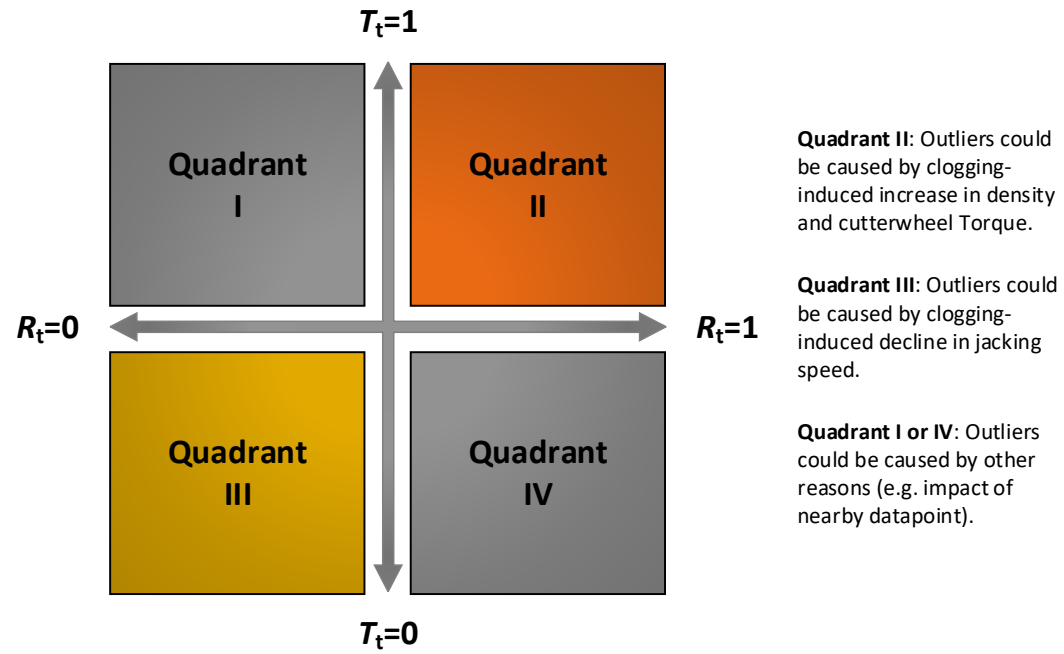


Fig. 17 Simple diagram for TBM operator to assess tendency to clayey clogging during slurry-supported pipejacking



(a)



(b)

Fig. 18 Clayey clogging with embedded gravel occurred while spanning through a ground composed of the clayey gravel and the gravel at drive
B: (a) before and (b) after the clay soil adhered to cutterwheel

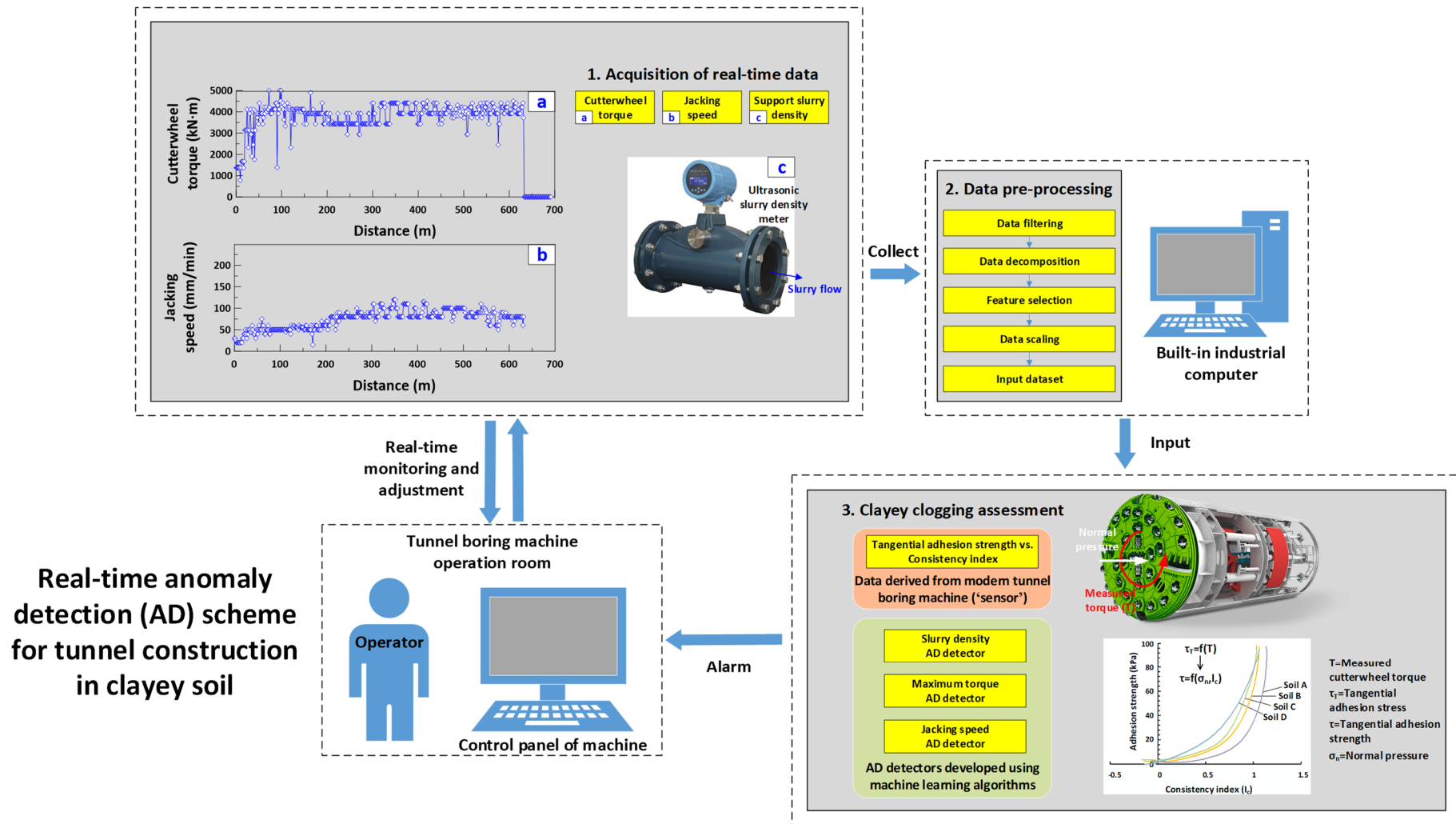


Fig. 19 Real-time anomaly detection scheme for tunnel construction in clayey soil